Solid state metathesis synthesis for ZnO-based materials towards applications in light-emitting diodes and ultra-violet-sensing devices

by

©TANZIR AHMED

A thesis submitted to the School of Graduate Studies in partial fulfillment of the requirements for the degree of

Master of Science

Department of Chemistry

Memorial University of Newfoundland

September 2018

St. John's Newfoundland

Abstract

Solid state metathesis (SSM) has gained much attention for the synthesis of ZnO-based semiconductors. SSM is a synthesis method that avoids organic solvents, high temperature calcination, and it is simple and fast. Co-doped ZnO has already been synthesized by several other methods (co-precipitation method, sol-gel). We wanted to use SSM to make Co-doped ZnO, in which Zn^{2+} ions are replaced by Co^{2+} ions. The thesis work goal was to prepare Co-doped ZnO to use it in light emitting diodes as a red light emitter. Raman spectra of the attempted Co-doped ZnO confirms the formation $Co(OH)_2$ as a secondary phase, which in turns converts into Co_3O_4 during high temperature calcination. There were no characteristic peaks in the visible region of UV-Vis spectra that would correspond to the emission of red light.

Stoichiometric ZnO films are good candidates for use in various sensing devices. The frequency-dependent UV response of SSM-produced ZnO films were studied under AC conditions. After storing in the dark for several days, the UV responses were studied by electrochemical impedance spectroscopy (EIS). The resulting data allow determination, for each individual film, what range of frequencies are appropriate for use in UV sensing.

Acknowledgements

I have the immense pleasure to express my deepest sense of gratitude and sincere appreciation to my supervisor Dr. Kristin M. Poduska for her supervision, invaluable suggestion, constructive guidance, continuous encouragement and mental support throughout the progress of this thesis.

I am grateful to my supervisory committee members Dr. Yuming Zhao and Dr. Bob Davis for their valuable advice and encouragement at the different stages of my research work.

I also express my perspicuous gratitude to my research group members for their heartiest co-operation and valuable advice.

School of Graduate studies, Memorial University of Newfoundland, Lumentra, Inc. (Toronto, Canada) and NSERC are greatly acknowledged for the financial support.

Table of Contents

List of Figures

List of Abbreviations and Symbols

AC	alternating current
ATR	attenuated total reflection
DC	direct current
DRS	diffuse reflectance spectra
E	potential
EIS	electrochemical impedance spectroscopy
IR	infrared
ITO	indium tin oxide
LED	light emitting diode
RGB	red, green and blue
S1	sample one
S2	sample two
S3	sample three
SSM	solid state metathesis
UV-Vis	ultraviolet–visible
WLED	white light emitting diode
Z	impedance
Z_{im}	imaginary part of impedance
Z_{re}	real part of impedance

e^-	electron
f	frequency
f_{cross}	frequency at crossing point
h^+	hole
ω	angular frequency
θ	changes of phase

Chapter 1

Introduction

Light obtained from light emitting diodes (LEDs) has a longer lifetime and higher energy efficiency. These attributes make them more economical than incandescent bulbs [1, 2, 6]. White light emitting diodes (WLEDs) can be made from phosphor materials, and even a small variation in phosphor colours can lead to a big change in the quality of lights. The use of different phosphors in controlling the color quality of white light is of particular interest to researchers [2].

1.1 Light emitting diodes

An LED is a light emitting device containing a chip at the center. An LED package may also have different phosphor materials in it that tune the outcoming light. Modification of the light from an LED package using a phosphor is known as phosphor method. Phosphors have luminescent properties, and they are mainly composed of transition metal or rare earth metal compounds by doping process [7]. Photons emitted from an LED chip, under the influence of electric voltage, interact with the phosphor materials and release light of a particular wavelength, which is very useful for lighting purposes. The colors of the light emitted by LED package can be modified

by using different phosphor materials because the right combination of an LED chip and phosphor influences the colors as well as the qualities of light emitted by the LED package [1, 2, 8]. Figure 1.1 illustrates the above process. Initially, a blue LED chip emits blue light. Photons from a blue chip excite the electrons of yellow phosphors, which results in luminescence emission as a yellow light. Photons that do not interact with the phosphor keep their original wavelength and proceed as a blue light. Finally, the yellow and blue light combine to produce white light [9].

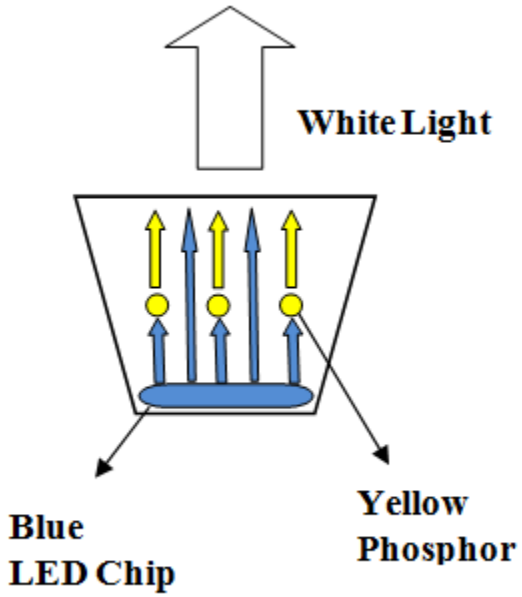

Figure 1.1: Phosphor method showing the process of getting white light from a LED package. Modified from Reference [1].

The white light can be classified as warm white, cool white or natural white based on its color temperatures [10,11]. The color can be tuned by adding different phosphor materials to the LED chip. Adding a red phosphor to the blue LED chip gives warm white light, also known as yellowish white with a color temperature around 3000 K [1, 2]. Another commonly known method to produce white light is RGB. Lights of three primary colors (red, green and blue) are mixed in a variety of ways and generate

a number of different colors.

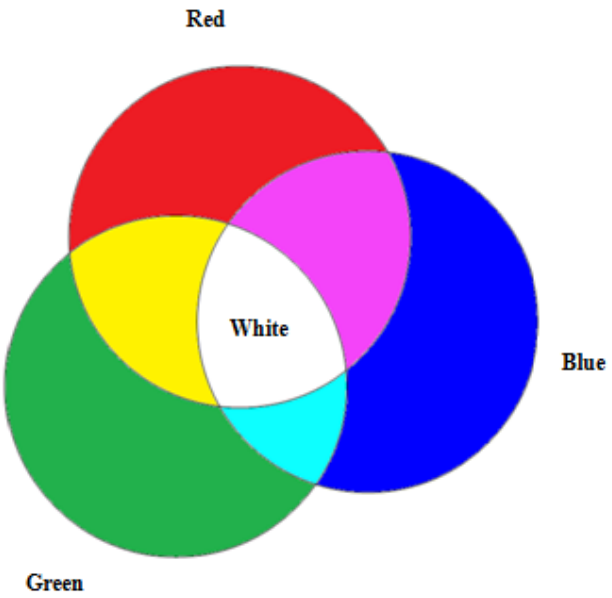

Figure 1.2: Mixing of different colors generates white light. This figure was modified from Reference [2].

Figure 1.2 depicts this process: the combination of red and blue produces magenta, whereas adding green to blue will create cyan. When red is mixed with green, we get yellow. White is achieved by mixing red, green and blue (RGB) [12].

1.2 Luminescent properties of phosphors

When phosphor materials interact with visible light, they absorb photons. Such absorption makes the electrons in the phosphor jump from the ground state to an excited state. However, electrons tend to occupy stable energy states. Thus, they leave the excited state and return to the ground state. During this return, they emit photons and lose energy in a process known as luminescence [7]. White light emitting diodes (WLEDs) contain luminescent materials. There are two ways in which light emission

occurs: fluorescence and phosphorescence [7, 13]. In fluorescence, the absorption and release of photons is a rapid and simultaneous process in which electrons return to their original state directly. On the other hand, after absorbing energy, it takes phosphorescent materials some time to emit light, since the return of an electron from an excited state to the ground state occurs *via* an intersystem crossing. Fluorescence is a radiative process, whereas phosphorescence takes two steps: an intersystem crossing is a non radiative process, and the last step occurs *via* a radiative process. When the light source is removed, phosphorescent materials emit light for a longer time than fluorescence materials [7, 13].

The mechanism of phosphorescence is commercially used in many materials, ranging from toys to clocks [7,14]. Likewise, the fluorescence mechanism (rapid emission of light) is widely used in many devices, such as LEDs, sensors and CRT monitors [15].

1.2.1 Luminescent properties of ZnO and Co-doped ZnO

ZnO is a transition metal oxide semiconductor. At room temperature, it is stable and forms an hexagonal wurtzite structure [16]. In hexagonal ZnO, all the O^{2-} ions are tetrahedrally coordinated with Zn^{2+} ions. Luminescence properties of ZnO largely depend on defects created during their synthesis. These defects can also stem from the incorporation of another element in the ZnO lattice [16]. They are of different kinds: intrinsic (zinc vacancies, oxygen vacancies, zinc interstitial, oxygen interstitial, antisites) or extrinsic defects [14, 17–20]. As a result of these defects, an additional energy level is created, thus impacting the luminescent property [21]. For instance, the emission of green light from ZnO occurs due to either oxygen and zinc vacancies [16, 22]. Oxygen vacancies and zinc vacancies are also responsible for the emission of red and blue light respectively, whereas, oxygen interstitials produce the emission of yellow light [21]. This type of emission makes ZnO appropriate to use in many optical

and electronic devices [23, 24].

Doping also leads to tuning the band gap energy of ZnO by modifying the energy of the valence and conduction band. The two most commonly used dopants, in this case, are transition metals [2, 25] and rare earth elements [2]. Among these, cobalt is frequently used as its valence states are quite similar to those of Zn [26]. Doping of Co into the ZnO lattice works in stage. First, Co^{2+} ions replace Zn^{2+} ions; afterwards, it creates defects in the ZnO lattice [26–36]. As a result of Zn^{2+} replacement by Co^{2+}, an orbital overlap occurs between Zn (4_s) and O (2_p) with Co (3d) [34, 37]. Thus dopants control the luminescence energy [34, 37].

Light producing devices such as LEDs can be fabricated by using the optical properties of ZnO and Co-doped ZnO. These materials can also be used in UV sensing devices [38, 39].

1.3 Methods used to synthesize ZnO and Co-doped ZnO

ZnO and Co-doped ZnO offer a wide range of applications in different domains of materials chemistry due to the fascinating properties of these materials. Different methods such as sol-gel, co-precipitation, hydrothermal, chemical and vapor condensation have been used for the synthesis of ZnO and Co-doped ZnO [38, 40–44]. In this research, a solid state metathesis reaction method was used because it does not require organic solvents or high-temperature calcination [42, 45]. On top of that, synthesis of different materials using this method is comparatively easy and requires less time [42, 45].

SSM methods been used for the synthesis of various kinds of materials such as metal nanoparticles, oxide materials, transition metal doped oxides, metal sulphides,

nitrides and phosphides [45–50]. Researchers have used SSM reactions to synthesize ZnO in order to study its optical, electrical and gas sensing properties [49–51]. Transition metal doped oxides were also prepared using the SSM method, where the optical properties of the materials were studied [45]. This material can also be used for the degradation of industrial dyes [45]. Muke *et al.* [51] synthesized rare earth doped $CaSO_4$ phosphor materials to use them in liquid crystal displays. In this study, Co doped ZnO was targeted with the SSM method to use it in LEDs as a phosphor.

1.4 Applications of ZnO in UV sensing devices

The exposure of ZnO and ZnO-based materials to different levels of light (daylight, UV light, and dark) affects their electrical properties [50,52]. This change in electrical behavior of materials under UV light triggers their applications in sensing and optoelectronic devices [50, 53]. Due to the wide (3.37 eV) and tunable band gap energy of ZnO compared to other semiconducting materials, they can detect UV light better than Si-based photodetectors [50, 52, 54–58]. Detection of UV light by ZnO can be based on response time, wavelength, incident light intensity or frequency [50, 57, 59].

ZnO can be used in UV sensing devices [39, 60–62]. Ambient oxygen and water influence the UV photoresponse of ZnO [3]. The photoresponse process of ZnO film depends on the environment and is controlled by the O_2 adsorption or desorption equilibrium at surfaces [3, 50, 63]. Under dark condition, when the film is dry, oxygen molecules are adsorbed in ZnO surface from the atmosphere and capture free electrons, thereby inhibiting their mobility. As the quantity of electrons decreases, the conductivity of ZnO declines with it.

$O_2(g) + e^- \rightarrow O_2{}^-(ad)$

Under UV illumination, ZnO absorbs photons and creates electron-hole pairs in

the bulk of ZnO.

$h\nu \rightarrow e^- + h^+$

These newly created holes move to the surface of ZnO and neutralize the previously adsorbed oxygen ions. In turn, the trapped electrons increase the conductivity of ZnO.

$O_2{}^-(\text{ad}) + h^+ \rightarrow O_2(\text{g})$

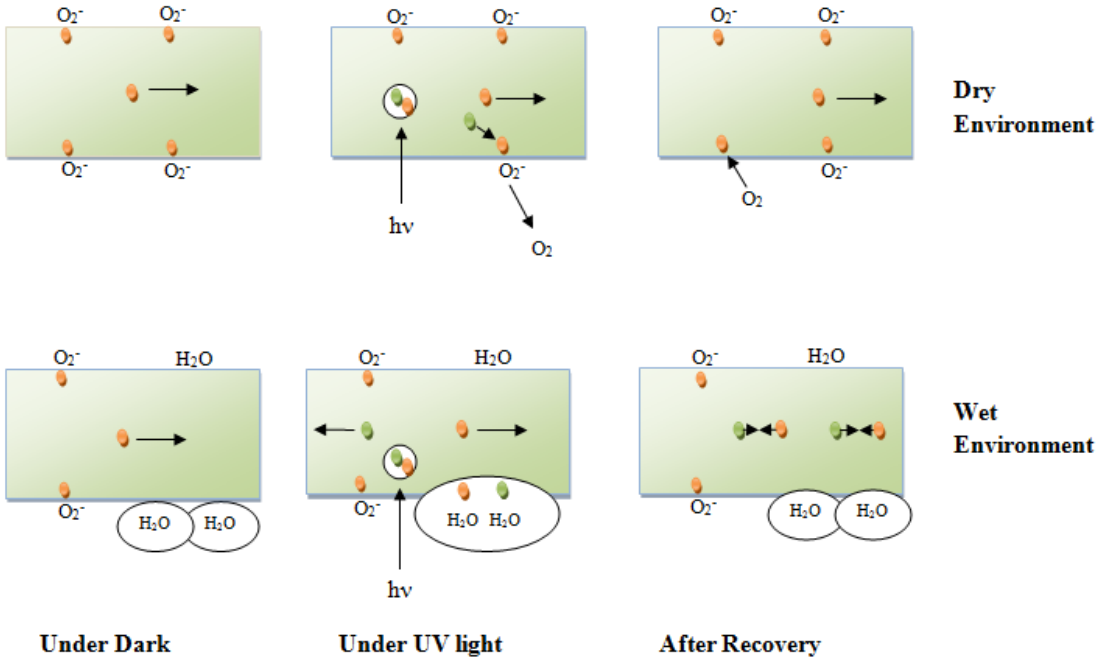

Figure 1.3: Photoresponse process of ZnO under wet and dry condition. This figure was modified from Reference [3].

Figure 1.3 shows how humidity affects the photoresponse behavior of ZnO sample. In a dark environment, water molecules replace the previously adsorbed oxygen ions on ZnO surface and free up the electrons, which increases ZnO conductivity. On the other hand, UV illumination creates electrons and holes that get trapped by water molecules. Fewer electrons reduce ZnO conductivity [3, 50]. Tewari *et al.* [64] studied frequency-dependent properties of Al-doped ZnO, whereas Martin *et al.* [65] investigated UV responses of ZnO film under DC and AC conditions.

In this thesis, the UV response of ZnO films under AC conditions was examined.

Shining UV light on a ZnO surface creates electron-hole pairs by absorbing photons of light. Generation of an electron-hole pair frees up electrons which decreases the resistance of the ZnO film [55, 66]. The resistance is known as impedance (Z) when it is in an alternating current (AC) circuit. In an AC circuit, the current that flows through the circuit changes cyclically because the input voltage varies with time. The polarity of AC changes from positive to negative direction and vice versa to complete a full cycle. Direct current (DC) does not change polarity. In this thesis work, we use electrochemical impedance spectroscopy (EIS) to apply an AC potential at a range of different frequencies to observe the impedance response of ZnO films.

UV sensing devices make use of a variety of semiconducting materials. Use of ZnO-based UV sensing devices is common in space communications, bio-medical devices, high-temperature plasma research, defense sector and in environmental sector [55]. Thin films of ZnO exhibit gas sensing properties [42, 64, 67]. Structure, band gap energy, stoichiometry and adsorbed gasses on ZnO surface determine the efficiency of ZnO-based UV sensor. Hence, controlling these properties of ZnO will help tune the performance of ZnO-based UV sensing devices [66, 68].

1.5 Overview of this thesis

In this thesis, a solid state metathesis reaction method was used to prepare Co-doped ZnO to determine its suitability for use in light emitting devices to modify the color quality of white light. The synthesis procedure of the samples is described in Chapter 2, as are the working procedures of different characterization techniques. The prepared samples were characterized by an attenuated total reflectance (ATR), Raman spectroscopy, and diffuse reflectance spectroscopy. The structural characterization and optical responses results are discussed in Chapter 3.

The photo-responsive behavior of ZnO films was also studied during this research. ZnO films were prepared on indium tin oxide (ITO) glass substrate by a drop casting method. The film preparation method and electrochemical impedance spectroscopy (EIS) measurement are discussed in Chapter 2 and 4. The conclusions of both two projects are written in Chapter 5.

The approach of this thesis work was to synthesize ZnO and Co-doped ZnO by using a simple and fast solid state metathesis reaction (SSM) followed by the study of their luminescent properties. In SSM, an ion exchange reaction occurs between two different precursors where both of them are in solid state [51,69]. The reaction product is found as a precipitate along with a soluble by-product. SSM reaction requires less energy to overcome the activation energy barrier which makes this reaction fast [69]. ZnO has a wide band gap energy (3.37 eV) that depends on the nature of defects in its lattice [16]. Those defects control the luminescent properties of ZnO. Defects can be created in the ZnO lattice during the synthesis process by doping different elements into ZnO [70]. The combination of band gap and defect emission falls in the range of visible region making it a very good choice for white light emitting diodes (WLEDs) [71, 72]. In contrast, Co-doped ZnO emits green or red light, which can be used in LEDs to enhance the quality of white light [2, 73].

To explore the suitability of ZnO films in making UV sensing devices, the study also focuses on their UV responsive properties.

Chapter 2

Experimental methods and characterization techniques

Synthesis methods of ZnO based materials have a significant impact on their properties. Therefore, the selection of a suitable method is important to get the desired product. Different spectroscopic techniques provide information about the composition and structural properties of ZnO as well as Co-incorporated ZnO samples. Diffuse reflectance spectroscopy gives the idea about the optical properties of those samples. Electrical measurements show the photoresponsive behaviour of ZnO films.

2.1 Chemicals

Zinc chloride hexahydrate ($ZnCl_2.6\,H_2O$) (Fisher Scientific, 97.2 %), cobalt chloride hexahydrate ($CoCl_2.6\,H_2O$)(ACP, 98 %), zinc nitrate hexahydrate ($Zn(NO_3)_2 \cdot 6\,H_2O$) (ACP, 98 %), cobalt nitrate hexahydrate ($Co(NO_3)_2 \cdot 6\,H_2O$) (Merck KGaA, 99 %), sodium hydroxide (NaOH, Sigma-Aldrich, 97 %) and ethanol (C_2H_5OH, ACP, 97 %) were used as received. All chemicals were analytical grade.

2.2 Solid state metathesis reaction

A solid state metathesis (SSM) reaction method was used to synthesize ZnO, $Co(OH)_2$ and Co-incorporated ZnO. Reaction between $ZnCl_2$ and NaOH was performed for the preparation of ZnO [49, 74].

$ZnCl_2 + 2NaOH \rightarrow Zn(OH)_2 + 2NaCl$, ΔH_f = -47.1 kcal/mol

$Zn(OH)_2 \rightarrow ZnO + H_2O$, ΔH_f = +13.2 kcal/mol

A schematic diagram of this process is given in Figure 2.1.

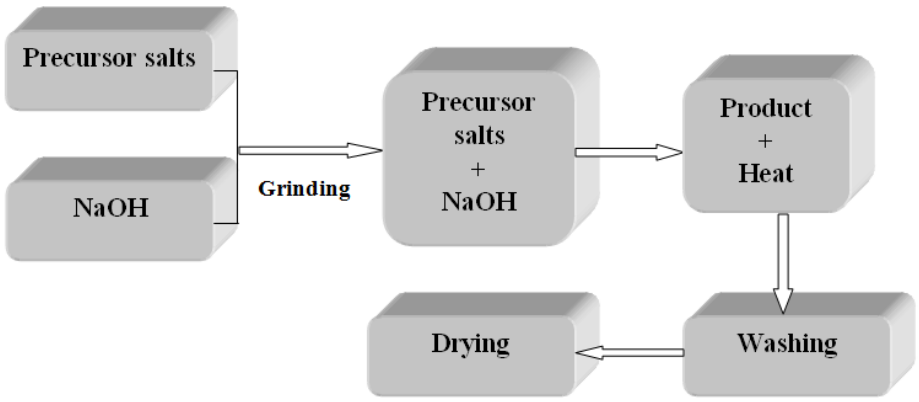

Figure 2.1: Schematic diagram showing the synthesis method for preparing ZnO-based oxides.

In SSM, precursor salts were ground with mortar and pestle. Ground powder was mixed in a beaker and stirred with a glass rod. The reaction products were washed with ultrapure water and dried at room temperature. Muhammad Asim Rasheed [49] has also mentioned in his PhD thesis that an SSM method for the synthesis of ZnO can be successful by using different precursor salts such as $Zn(NO_3)_2$ and $ZnSO_4$. A reaction scheme of two salts for the preparation of ZnO is presented below:

$Zn(NO_3)_{2(s)} + 2NaOH_{(s)} \rightarrow Zn(OH)_{2(aq)} + 2NaNO_{3(aq)}$

$Zn(OH)_{2(aq)} \rightarrow ZnO_{(s)} + H_2O_{(l)}$

Reactions between $ZnSO_{4(s)}$ and $NaOH_{(s)}$ are as follows:

$ZnSO_{4(s)} + 2NaOH_{(s)} \rightarrow Zn(OH)_{2(aq)} + Na_2SO_{4(aq)}$

$Zn(OH)_{2(aq)} \rightarrow ZnO_{(s)} + H_2O_{(l)}$

SSM reactions have the advantages that they avoid organic solvents and high-temperature calcination.

2.3 Synthesis of ZnO, $Co(OH)_2$ and Co incorporated ZnO *via* solid state metathesis reaction

A solid state metathesis reaction method was used for the preparation of ZnO nanoparticles [49, 74]. For the synthesis of ZnO, 2.04 g of $ZnCl_2 \cdot 6\,H_2O$ and 1.18 g of NaOH were used, and they were ground with mortar and pestle for 10 minutes. The ground powders were mixed in a beaker and stirred with a glass rod for 1-2 minutes. A very fast reaction with fuming occurred. The product was formed as a white slurry, which was washed several times with ultrapure water so that the by-product, NaCl, could be removed. The white slurry of ZnO was then dried at room temperature in the fume hood for 12 hours.

Another set of SSM reaction (with different weight ratios of precursors) was used in an attempt to obtain Co-doped ZnO, with precursor salts, $ZnCl_2 \cdot 6\,H_2O$ and $CoCl_2 \cdot 6\,H_2O$. The room temperature drying turned the sample to light green. Different amounts, 2, 4, 6, 8 and 10 wt.% of the $CoCl_2 \cdot 6\,H_2O$ precursor, were used.

In the case of Co doping into ZnO, secondary phases are formed quite often. In order to explore the possibility of formation of such secondary phases, an SSM reaction between $CoCl_2 \cdot 6\,H_2O$ and NaOH was performed with the molar ratio of 1:2, in which 1 g cobalt chloride hexahydrate ($CoCl_2 \cdot 6\,H_2O$) and 0.336 g of NaOH were ground for 10 minutes with a mortar and pestle. The reaction between $CoCl_2 \cdot 6\,H_2O$ and NaOH formed a blue colored slurry, which immediately turned into a light purple slurry.

After being stirred with a glass rod, the product was washed with ultrapure water. The product was then filtered and dried at room temperature in the fume hood.

2.4 Preparation of ZnO films

ZnO powder was prepared by an SSM method, then washed with ultrapure water. After drying at room temperature, it was calcinated at 500 °C for 5 hours. A slurry of ZnO was prepared by mixing 0.1 g of ZnO powder and 2 ml of ethanol/water solution.

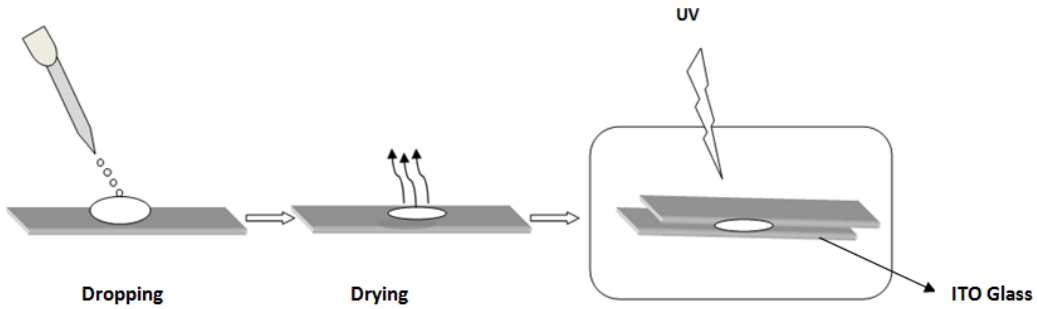

Figure 2.2: Preparation of ZnO film on ITO glass substrate by drop-casting method.

To prepare a homogeneous solution of ZnO, the slurry was sonicated for 30 seconds. ITO glass was used as a substrate to make films of ZnO on it. A slurry of ZnO was placed on an indium tin oxide (ITO) glass substrate by a drop casting method, which is presented in Figure 2.2.

2.5 Controlling moisture of ZnO films

Under ambient conditions, water (humidity), impurities and other gas molecules can interact with the surface of ZnO which influences the photoresponse properties of the ZnO film. The interaction mechanism between foreign materials and the ZnO surface is not straightforward. Better understanding and more research are required to find

a proper way of minimizing this kind of impact on photoresponse of ZnO. This study was focused only on the effect of humidity on photoresponsive properties of ZnO. Adsorption of the water molecules on ZnO surface causes the decrease of resistance of the ZnO film [3, 75].

The ZnO sample was stored in a box (a dimension of 14 cm length, 14 cm width and 14 cm height) with a bulk amount of activated desiccant in it. Desiccants were used to reduce humidity from the sample and they were activated on a daily basis. Desiccants are hygroscopic and turn pink after absorbing moisture. Desiccants were regenerated by microwaving for 3-5 minutes and left for a while to get back to their original red color.

2.6 Raman spectroscopic measurements

Raman spectroscopy uses a beam of laser light with a particular wavelength that interacts with the material [76, 77]. This interaction causes the scattering of light. The scattering can take place either elastically or inelastically, which is presented in Figure 2.3. In case of elastic scattering (Rayleigh scattering), the wavelength of incoming light does not change after the interaction with the material. Inelastic scattering is known as Raman scattering, where the energy of the scattered light can be greater or less than the incident light. If the energy of the incident light is greater than the scattered light, then this situation is called Stokes scattering. However, in the case of anti-Stokes, the incident light comes from an upper vibrational level rather than the ground state, and the scattered light reaches the ground state. Thus, the energy of the incident light is smaller than that of the scattered light. The change of energy between scattered and incident photon is called a Raman shift, which is used to produce a Raman spectrum of the material. Raman spectra provide some information

that can be used for the characterization of materials and the identification of defects in the crystal structure [76, 78].

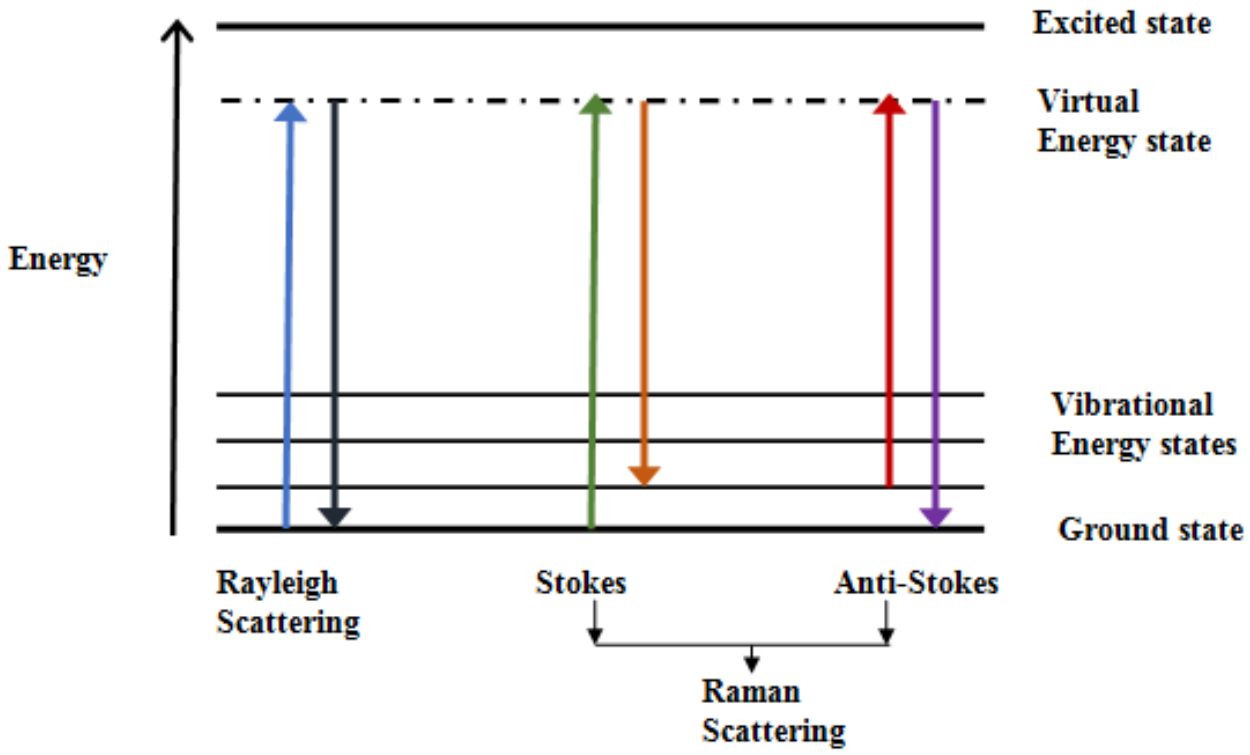

Figure 2.3: The energy-level diagram of Rayleigh scattering and Raman scattering showing the energy differences between the incident and scattered photons. This diagram was modified from Reference [4].

The Raman spectra of ZnO, along with the mixed phases of Zn and Co-containing precursors, were taken using a Renishaw inVia Raman microscope, to obtain information about the structures and effects of impurity doping in the host lattice. Samples were irradiated with a laser beam with an excitation wavelength of 830 nm.

Before starting the sample measurements, it is essential to calibrate the frequency of the Raman spectrometer, because this improves the accuracy of the spectra. A silicon wafer bar is usually used as the standard for the calibration because silicon avoids fluorescence and the photobleaching effect. The silicon standard was placed

under the objective lens, and focusing was performed manually by adjusting the distance between the objective lens and the sample. An octagonal shape was observed from the microscopic eyepieces. At this point, changing the mode of the spectrometer from the light mode to the laser mode gives a laser spot at the center of the cross-hairs on the computer screen. The position of the silicon bar can be adjusted by using a joystick. A 50 X objective lens and 100 percent laser power were used for calibration. A sharp peak of 520 cm^{-1} indicates accurate calibration.

The sample was dried and ground to obtain a fine powder. A small amount of the sample was placed on a clean glass substrate which was mounted on a sample stage. After each measurement, the glass substrates were wiped and cleaned with ultrapure water. A Leica confocal microscope was used with a 20 X objective lens. Focusing was done by adjusting the distance between the sample and the objective lens. The correct combination of laser power and acquisition time provides accurate Raman spectra. The Raman system has a maximum laser power at 100 % of 300 mW. The ZnO (white) sample gives good Raman spectra (high signal to noise ratio) at a higher laser power (50 %). On the other hand, in the case of Co_3O_4 (black), better Raman spectra was obtained at a low laser power (<1 %). Mixed samples (Co-Zn) of the precursors give the best Raman spectra at laser power between 1-10 %. The use of very high laser power makes it very difficult to focus on the sample. The samples were measured in the range of 100 cm^{-1} to 3200 cm^{-1}. Raman spectra were taken from different parts of the sample. There was no evidence of the sample burning upon interaction with the laser light.

2.7 Attenuated total reflection-infrared measurements

The infrared (IR) beam passes directly through the sample in a transmission IR spectrometer. However, in case of an attenuated total reflection (ATR) IR spectrometer, the IR beam is incident at a certain angle. The real part of the incident beam is reflected. The imaginary part (the evanescent wave) penetrates through the surface of the crystal to the sample (mounted on the ATR crystal), followed by the reflection of the wave from the sample. This evanescent wave then becomes attenuated due to the IR absorption by the sample. The attenuated evanescent wave then reflects back and reaches to the detector at the other side of the crystal which gives the spectrum of the sample [5]. Figure 2.4 describes the above process.

To obtain a better reflection of the evanescent wave, it is important to maintain a good contact between the sample and the crystal. ATR spectroscopy can be used to identify standard differences among samples [5].

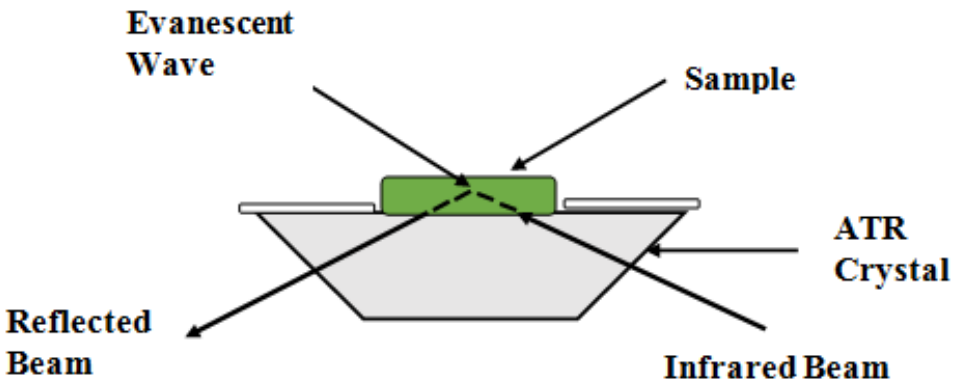

Figure 2.4: Geometry of ATR-FTIR beam path. Modified from Reference [5].

A Bruker Alpha ATR-IR spectrometer was used to get the spectra of ZnO based materials. A background measurement was done before sample measurements. The

samples were ground to obtain fine powder and were placed on the diamond crystal by keeping good contact with the help of a pressure clamp. The platform of the spectrometer was cleaned with ultrapure water before measuring the sample. The sample was measured in the range of 365 cm^{-1} to 4000 cm^{-1} with 24 scans.

2.8 Diffuse reflectance spectroscopy

Diffuse reflectance spectroscopy (DRS) is an effective characterization technique used for the analysis of solid state materials. From the reflectance spectra of materials, it is possible to determine the band gap energy by locating the wavelength at which a sudden drop of the absorption spectrum begins (absorption edge) [50].

An Ocean Optics DT 1000 CE spectrophotometer, containing a dual prolonged fiber optic cable with a light emitter and a light sensor, was used to take the UV-Vis diffuse reflectance spectra of Co and Zn containing mixed oxide samples. The light sensor portion is connected to the UV-Vis light source and the light emitting portion to the USB 2000 spectrometer. The end of the fiber optic probe was placed at a 45^o angle entry point of a black probe holding block. To minimize the interference of external light, the fiber optic probe and the holding block was kept in a wooden box.

SpectraSuit software was needed to acquire the UV-Vis spectra. The range of the USB 200 Spectrometer was 178.3 - 877.6 nm. An Ocean Optics perfect reflector was used as a reference standard. The reflectance of the sample was obtained with respect to the reflectance of the white reference bar, which gives close to 100 percent reflectance. The white surface of the reference standard was placed under the probe at the 45^o entry point. The room light was turned off, and the UV-Vis light source was turned on before starting the measurement. Some parameters (Integration time 200 ms, Scans to average 1 and Box Car Width 5) on the SpectraSuit software needed

to be set for the acquisition of god data. The light reference spectrum, as well as the dark reference spectrum, were recorded. After this stage, the diffuse reflectance spectra of the samples can be measured. The samples were placed in between two glass slides and kept under the probe to obtain reflectance of the sample. The probe was placed at different parts of the sample.

2.9 Observations of luminescent properties

The goal of this project was to prepare Co-doped ZnO that will emit red light. To obtain a preliminary idea about the luminescent properties, the samples were placed under a UV lamp to see the emission of light from the sample. A ENTELA UVGL-25 model compact UV lamp was used to check for evidence of light emitted from the sample. However, no emission of light was observed in our sample.

2.10 Electrochemical impedance spectroscopy

This Section describes how ZnO films respond to an AC potential. An EIS measurement is used to determine the impedance (Z) of a system, which is measured by applying an AC potential at a certain frequency. A Princeton Applied Research Potentiostat/Galvanostat (model number 273A), connected to a lock-in amplifier (Signal Recovery Model 5210), was used to measure the impedance. Power SUITE software was used to display EIS data.

EIS works on a principle where a small AC potential is introduced to the sample. Its response is measured over a range of frequencies and explained by a complex exponential function. This exponential function has a real and an imaginary part [50, 79–81].

An applied AC potential to the electrode can be expressed mathematically as [80]:

$$E_t = E_0 \, sin \, \omega t \tag{2.1}$$

where, E_t is the potential, E_o is the amplitude of the signal, and ω is the angular frequency.

The relationship between angular frequency ω and frequency f is:

$$\omega = 2\pi f \tag{2.2}$$

The outcome of the applied potential, i.e. the current, I_t, can be written as:

$$I_t = I_o \, sin \, (\omega t + \theta) \tag{2.3}$$

where, θ is the changes of phase after applying a potential to the system.

The voltage and current obtained from Equation 2.1 and 2.3 are then represented against frequency through Fourier transformation. The above equations were used to get the impedance, $Z\,(\omega)$, which is a complex number

$$Z\,(\omega) = \frac{E_t}{I_t} = \frac{E_0 \, sin \, \omega t}{I_0 \, sin \, (\omega t + \theta)} = \frac{Z_0 \, sin \, \omega t}{sin \, (\omega t + \theta)} \tag{2.4}$$

The impedance, $Z\,(\omega)$, has a real part Z_{re} and an imaginary part Z_{im} part, which can be expressed by the following equation:

$$Z\,(\omega) = Z_{re} \; + jZ_{im} \tag{2.5}$$

The exponential form of complex numbers in Equation 2.4 can be written using Euler's formula:

$$Z\,(\omega) = \frac{E_0 \, exp \, (j\omega t)}{I_0 \, exp \, (j\omega t - \theta)} = Z_0 \, exp \, (j\omega) \tag{2.6}$$

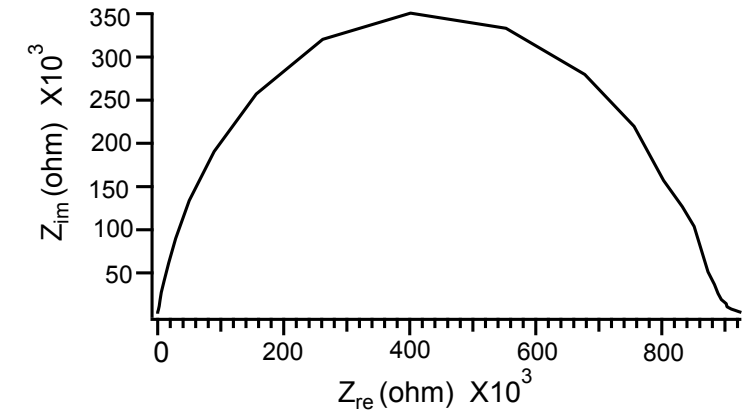

(a) Nyquist plot of ZnO film measured under dark

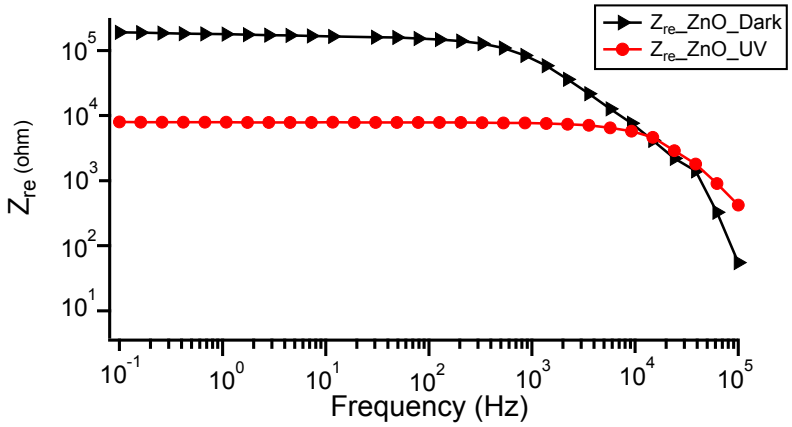

(b) Bode plot of ZnO film measured under dark and under UV light.

Figure 2.5: Nyquist and Bode plots of a ZnO film measured under UV and dark conditions

Equation 2.6 can also be expressed as:

$$Z\left(\omega\right) = Z_0\, exp\left(j\omega\right) = Z_0\left(cos\,\theta + jsin\,\theta\right) \tag{2.7}$$

The obtained data from the EIS measurements can be represented graphically in two forms, which are known as Nyquist and Bode plots (Figure 2.5).

.

In the Nyquist plot, the real part of the impedance, (Z_{re}) is plotted against the

imaginary part, (Z_{im}), where the impedance is measured at each frequency [50, 81]. In the case of a dry sample, the Nyquist plot forms a semi-circle, but if the sample is not perfectly dried, a 45 ^{o} phase shift is observed at low-frequency region [81]. This shift looks like a tail which is due to diffusion of ions. It is also known as Warburg impedance [81].

Another way of interpreting EIS data is to use a Bode plot where the change of impedance of the sample is measured at different frequencies. EIS data can be modeled with an equivalent circuit. The equivalent circuits help to identify contributions due to resistive and capacitive effects in the ZnO film [50, 79].

Chapter 3

Synthesis and characterization of Zn- and Co- containing powders

Choosing the right method and reaction conditions are very important for the synthesis of Co-doped ZnO. Due to the fast and solvent free nature, solid state metathesis (SSM) was used for the synthesis of ZnO as well as Co-incorporated ZnO. Selection of precursor salts and weight ratio has an influence on doping of Co into ZnO. Secondary phases are found quite often during this process of Co-incorporation into ZnO. Heat treatment was done to identify the secondary phases. Incorporation of Co into ZnO lattice gives the presence of secondary phases, which was observed by Raman spectroscopic measurements. UV-Vis diffuse reflectance spectra of Co-incorporated ZnO samples were taken by diffuse reflectance spectroscopy (DRS) to find the presence of peaks that were expected for red emission. However, there was no evidence of such emission.

3.1 Synthesis of ZnO particles

The white ZnO powder obtained by SSM reaction, described in Section 2.3, was dried at 80 °C in an oven for 6 hours. Raman spectra of the ZnO powder were taken in the range of 100-1200 cm^{-1}.

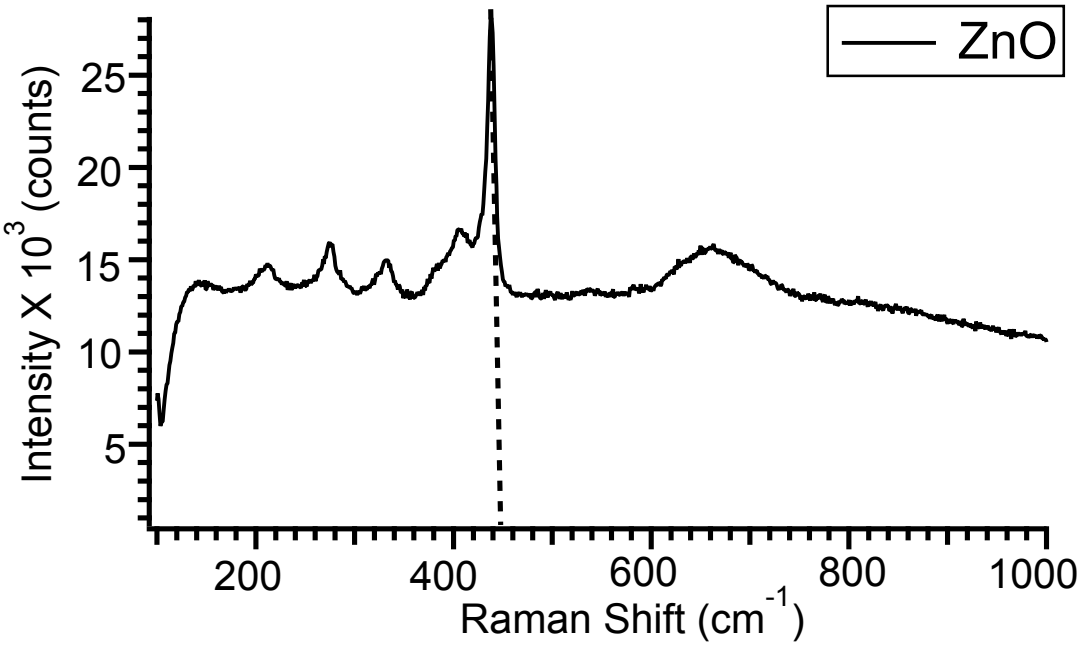

Figure 3.1: Raman spectrum of ZnO powder, dried at 80 °C. The dashed line shows the main peak expected for ZnO.

The Raman peaks of ZnO presented in Figure 3.1 are consistent with the literature [82–84].

3.2 Solid state metathesis reaction for cobalt oxides synthesis

The light purple sample prepared by SSM method, described in Section 2.3, was heated in an oven at different temperatures so that the color changes and structure

changes could be observed. The sample dried at 60 °C for 6 hours did not show any significant change in color, but turned into black when it was dried at 200 °C for 6 hours. Raman spectroscopic measurements of the samples were performed to obtain structural information from the synthesized products.

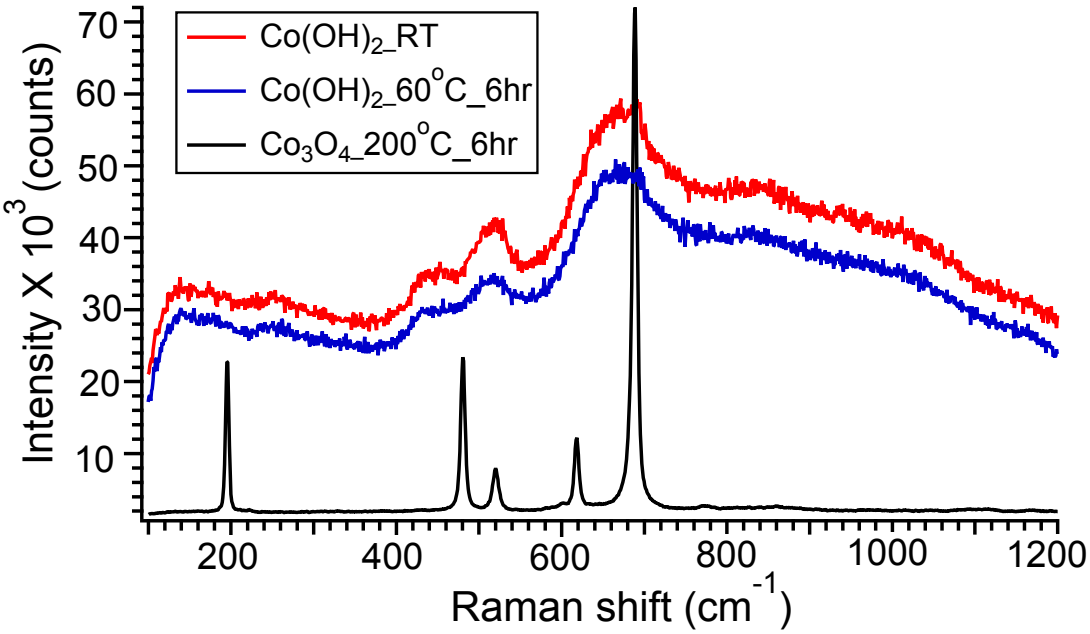

Figure 3.2: Raman spectrum of $Co(OH)_2$ showing the effect of heating. Heating the sample at 200 °C leads to the formation of Co_3O_4.

Raman spectra in Figure 3.2 show that samples dried at room temperature and 60 °C give peaks at identical positions. According to the literature [85], the Raman peaks that appeared for these samples are due to the formation of $Co(OH)_2$. The sample was also heated at 200 °C in an oven for 6 hours and formed a black powder. The Raman peaks obtained from this black sample are similar to the Raman spectra of Co_3O_4 [86, 87]. Therefore, heating the sample at 200 °C converts $Co(OH)_2$ into Co_3O_4.

Based on the literature, [88, 89] phases such as cobalt oxyhydroxide (CoOOH) and $Co(OH)_3$ can form during the conversion of $Co(OH)_2$ to Co_3O_4. The Raman

spectra of our products were compared with the intermediate oxides obtained from the literature, they are quite different from the spectra of $Co(OH)_2$ and Co_3O_4. Thus, our products do not contain cobalt oxyhydroxide (CoOOH) or $Co(OH)_3$.

The attenuated total reflectance (ATR) spectrum of the room temperature dried sample was taken to reconfirm the presence of -OH group in $Co(OH)_2$, which was then compared with the ATR spectrum of the heated $Co(OH)_2$.

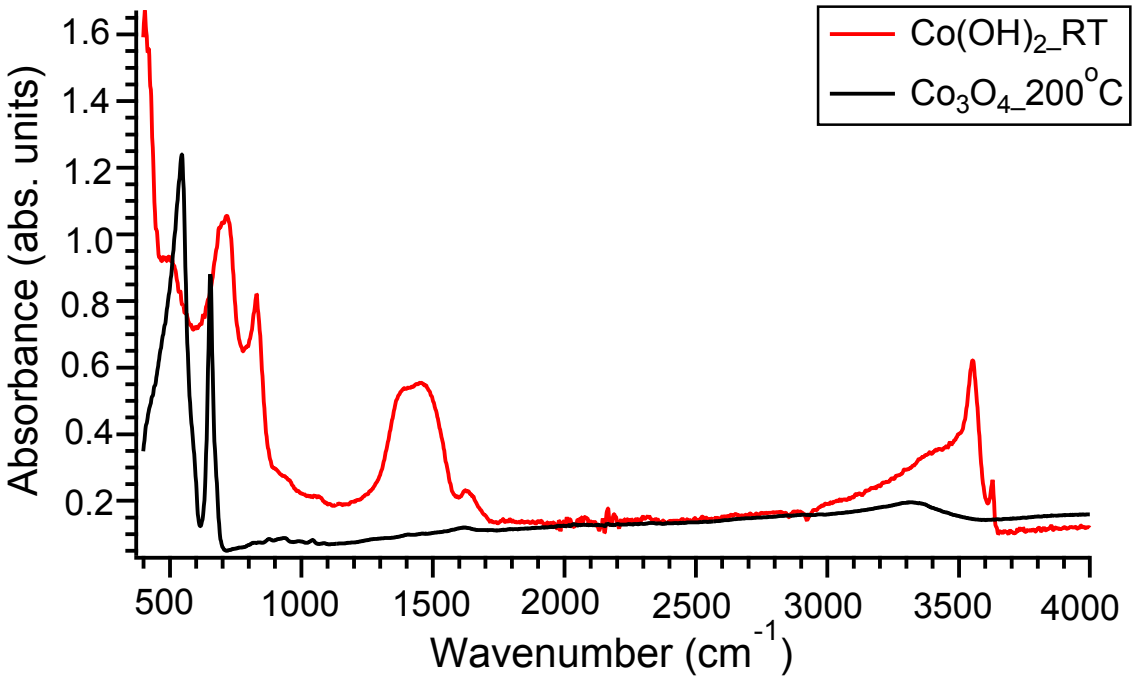

Figure 3.3: ATR spectra of $Co(OH)_2$ sample after drying it at room temperature and at 200 °C.

The ATR spectra in Figure 3.3 show the comparison between room temperature dried $Co(OH)_2$ and heated $Co(OH)_2$ samples. The ATR spectra of the room temperature dried sample showed two distinctive peaks at around 513 cm^{-1} and 3556 cm^{-1}, which are due to Co-OH bending and stretching respectively [85, 90, 91]. The formation of Co_3O_4 was confirmed by the two peaks of the heated sample at around 547 cm^{-1} and 665 cm^{-1} [92, 93].

3.3 Solid state metathesis reaction and optical properties of mixed Co and Zn salts

Raman measurements of mixed transition metal samples, synthesized according to the procedure described in Section 2.3, were done to investigate the structural properties. Raman spectra of Co-incorporated samples with different weight ratios are presented in Figure 3.4.

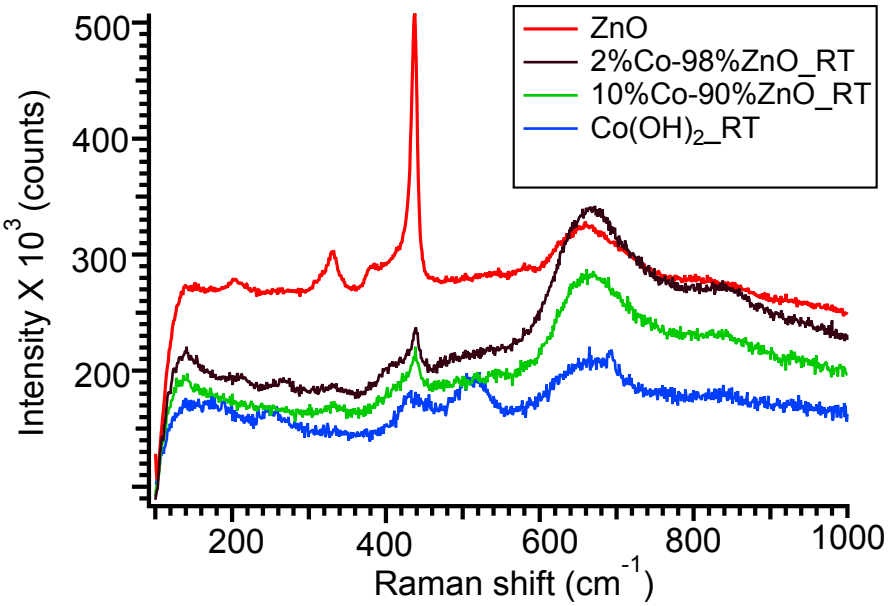

Figure 3.4: Raman spectra of Co-incorporated ZnO with different ratios of Co and Zn, dried at room temperature. The $Co(OH)_2$ spectrum is also shown for comparison.

Figure 3.4 shows that all of the mixed samples have Raman bands that resemble the ZnO sample. The presence of $Co(OH)_2$ as the secondary phase is not very clear, since the two Raman peaks of $Co(OH)_2$ at 430 cm^{-1} and 673 cm^{-1} are in similar positions to those of ZnO. Bhargava *et al.* [94] mentioned that the two Raman peaks at 551 cm^{-1} and 718 cm^{-1} should appear in Raman spectra of Co-doped ZnO; however, no such peak was found in that region.

Annealing heightens the Raman peaks, which makes it easier to tell what phase(s)

are present. Some powder was heated at 60 °C for 5 hours to see the appearance of possible secondary phases. The sample heated at 60 °C did not show any significant change in color. The green colored product remains the same after drying it in an oven at 60 °C for 5 hours. Raman measurements of these samples were done to see possible structural changes as well as to look for the presence of secondary phases in the sample.

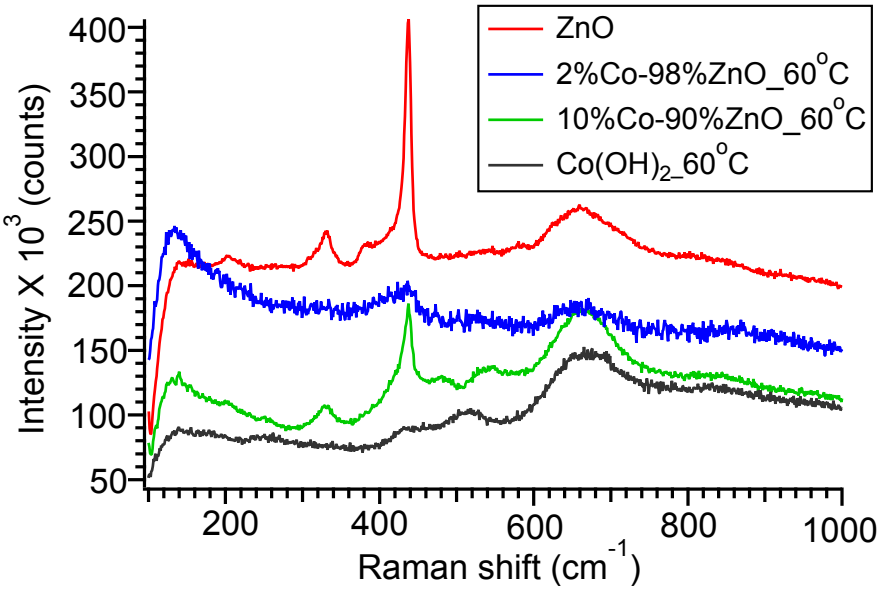

Figure 3.5: Raman spectra of mixed precursors of Co and Zn dried at 60 °C. Samples heated at 60 °C have no change in their Raman spectra.

Figure 3.5 shows that heating at 60 °C does not create any change in the sample. At this stage, the formation $Co(OH)_2$ was unclear as a secondary phase.

Since it is known that at high-temperature $Co(OH)_2$ converts to Co_3O_4 [95], the samples were also heated at 200 °C, and Raman spectra of the heated samples were taken to observe the possible conversion of $Co(OH)_2$ to Co_3O_4.

Figure 3.6 shows the Raman spectra of Co-incorporated ZnO with different concentrations of Co. The Raman spectra of mixed samples provide peaks which are identical with the peaks of ZnO. Along with the formation of ZnO, additional Raman

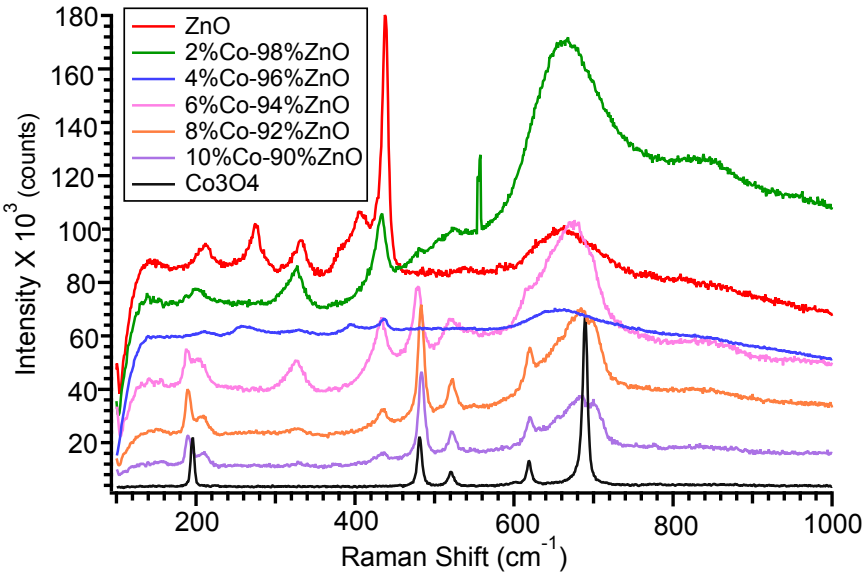

Figure 3.6: Raman spectra of mixed precursors of Co and Zn showing the effect of different concentrations of cobalt precursors, after heating at 200 °C. Samples with different concentrations give peaks at similar positions.

peaks were also found, which are similar to the Raman spectra of Co_3O_4 [86,87]. The broadening and weakening of the main peaks of ZnO were not observed which is the indication of unsuccessful Co-doping. Raman study of Co-incorporated ZnO suggests that instead of Co-doping into ZnO, $Co(OH)_2$ and Co_3O_4 formed as secondary phases in the sample at lower and higher temperatures, respectively. Evidence of formation of Co_3O_4 as a secondary phase is clearer at higher concentrations of cobalt. These might be due to the higher amount of cobalt precursors added to the ZnO.

The addition of Co into ZnO would cause a new feature in the UV-Vis spectrum because in a doping process, Zn^{2+} ions are replaced by Co^{2+} and forms defect into ZnO lattice [44]. In case of Co-doped ZnO, three different peaks come in UV-Vis spectra due to the d-d electronic transitions in Co^{2+} [33, 34, 96]. UV-Vis reflectance spectra of 2 wt.% and 10 wt.% samples were taken. The comparison of these spectra with the spectra of raw white standard and ZnO is presented in Figure 3.7.

UV-Vis reflectance spectra of room temperature dried sample in Figure 3.7. show

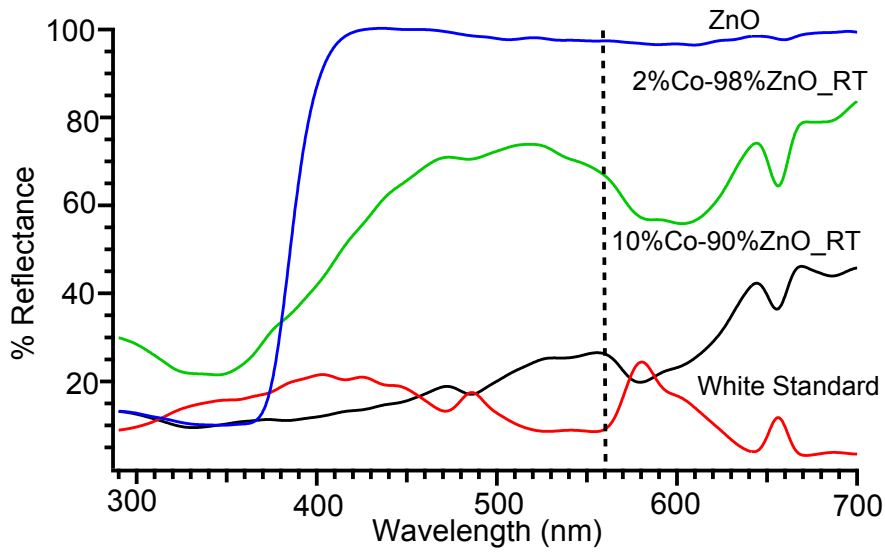

Figure 3.7: Diffuse reflectance spectra of Co-incorporated ZnO, dried at room temperature. Positions of the peaks are indicated by the dashed line.

a very weak and broad peak at around 568 nm, which was observed in the visible region of UV-Vis spectra. This peak originates from the green sample. Successful doping of Co into ZnO gives a peak at around 658 nm, giving red emission [33,34,96]. Conversely, peaks were observed at this position that are identical with the peaks of the white standard. Thus, it suggests that there was no doping of Co into ZnO at room temperature. The direction of the sample peaks are opposite to those of the standard, which is due to the subtraction of the peaks from the standard.

According to the literature, [35,36,97–103] the color of the Co-doped ZnO is green. Hays *et al.* [33] synthesized Co-doped ZnO by the sol-gel method. In their synthesis, they used very low concentration of Co precursors heated at 350^{o}C. We hoped that heating the samples would show more clearly whether we had multi-phase products. So, we heated our samples at 200 ^{o}C for 5 hours in an oven, which gives them a deep green color. Figure 3.8 presents the images of Co-incorporated ZnO samples with different weight ratios. The color of the samples became darker with higher Co concentrations. This is similar to what Hays *et al.* [33] observed.

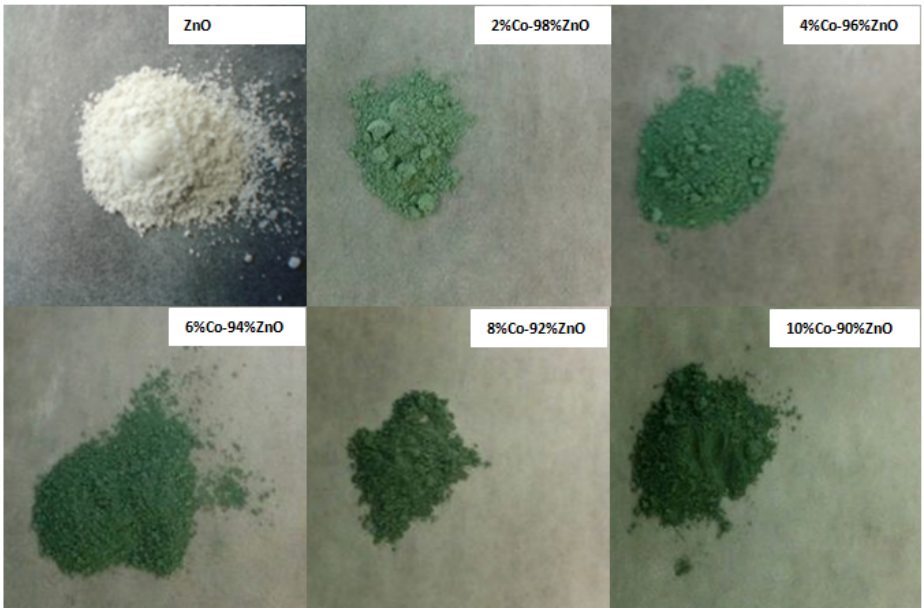

Figure 3.8: Color photos of ZnO and mixed phases of Co and Zn precursors heated at 200 °C.

UV-Vis reflectance spectra of heated Co-incorporated ZnO samples were measured and then compared with the white standard and ZnO.

UV-Vis reflectance spectra in Figure 3.9 also show the presence of peaks at around 568 nm and 658 nm in the visible region. The peak at around 568 nm comes from the green sample, and the peak at 658 nm arises because of the white standard. The Co concentration and the amount of heat do not have any influence on the spectra. The lowering of reflectance with increasing the concentrations of cobalt was observed, which is consistent with its darker color.

As mentioned above, [33, 34, 96] Co-doping into ZnO would be confirmed by the appearance of peaks in the visible region, especially a peak that is responsible for red emission at around 658 nm. However, the characteristic peaks in the UV-Vis reflectance spectra were not observed. Doping can also be confirmed by determining the band gap energies of samples. A change in band gap energy could not be detected because the spectra have the same reflectance shoulder position at 365 nm.

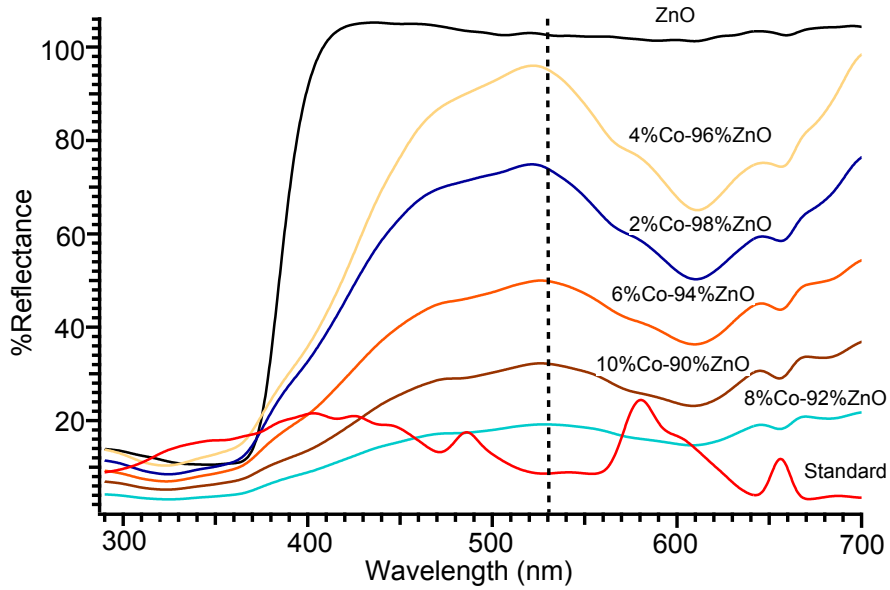

Figure 3.9: Diffuse reflectance spectra of Co-incorporated ZnO measured after heating at 200 °C. The dashed lines show peaks expected if Co were incorporated into the ZnO lattice.

Finally, samples were placed under a UV lamp to see if there was an emission of light. However, no emission of light was observed. Therefore, the solid state metathesis reaction method did not work well for Co-doping into ZnO.

Upon successful doping of Co into ZnO, the main Raman peak of ZnO becomes weaker and broader, both are the evidence of the destruction of the ZnO lattice structure [94, 104–106]. In order to know whether there is any Co-doping (or not), the changes of the appearance of this peak were observed.

3.4 Solid state metathesis reaction of mixed Co and Zn with different precursor salts

Selection of precursor salts has a significant effect in Co-doping into ZnO [94]. Bhargava *et al.* [94] used three different precursors, such as cobalt chloride hexahydrate

$(Co(Cl)_2 \cdot 6\,H_2O)$, cobalt acetate tetrahydrate $(Co(CH_3COOH)_2 \cdot 4\,H_2O)$ and cobalt nitrate hexahydrate $(Co(NO_3)_2 \cdot 6\,H_2O)$ to obtain secondary phase free Co-doped ZnO. Along with successful doping, they also have found that Co_3O_4 formed as a secondary phase [94]. In this thesis, $Zn(NO_3)_2 \cdot 6\,H_2O$ and $Co(NO_3)_2 \cdot 6\,H_2O$ were used as new precursor salts, and an SSM reaction between those precursors was carried out to obtain Co-incorporated ZnO by changing the amounts.

An SSM reaction between 2 wt.% $Co(NO_3)_2 \cdot 6\,H_2O$ precursor and 98 wt.% $Zn(NO_3)_2 \cdot 6\,H_2O$ precursor gives a white slurry, immediately after mixing with NaOH. Similarly, the reaction between $Zn(NO_3)_2 \cdot 6\,H_2O$ and $Co(NO_3)_2 \cdot 6\,H_2O$ was performed where 10 wt.% of cobalt precursors were used to see the possibility of doping by changing the amount of the precursors. In both cases, a white slurry was obtained as a product, which was then washed and dried at room temperature. The samples were then characterized by Raman spectroscopy. The Raman spectra of those samples are presented in Figure 3.10.

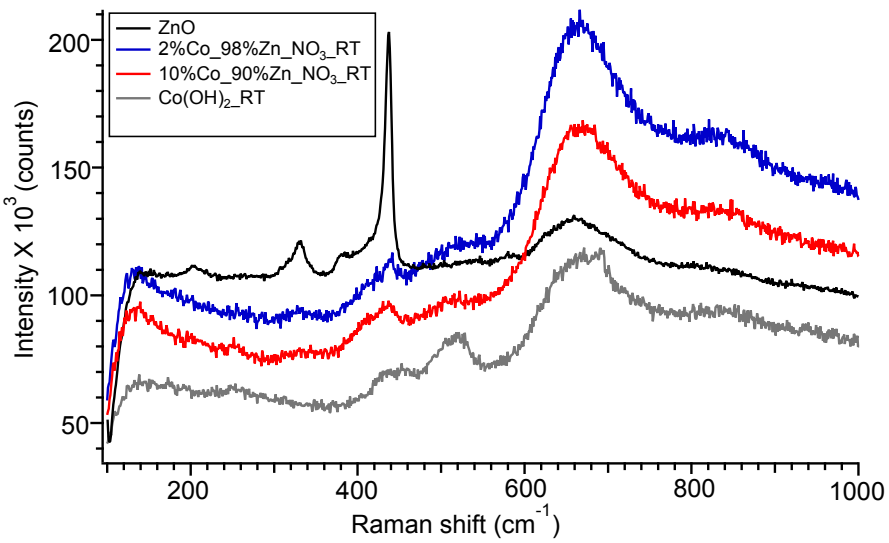

Figure 3.10: Raman spectra of mixed Co and Zn phases obtained using NO_3 salts as precursors. All samples were dried at room temperature.

Raman spectra in Figure 3.10 show that Co-incorporated ZnO using $Zn(NO_3)_2 \cdot 6\,H_2O$

precursor gives identical Raman peaks of ZnO. In this case, also, Raman peaks at 551 cm^{-1} and at 718 cm^{-1} were not found, an indication of unsuccessful doping of Co into ZnO. Raman spectra did not show clear evidence of the presence of $Co(OH)_2$, as an expected secondary phase.

The samples were then heated at 325 °C because $Co(OH)_2$ converts to Co_3O_4 at higher temperature [95]. A green product was obtained after drying at room temperature, but it was changed to deep green after heating at 325 °C. Afterwards, Raman spectra were collected to identify the formation of a secondary phase in the sample.

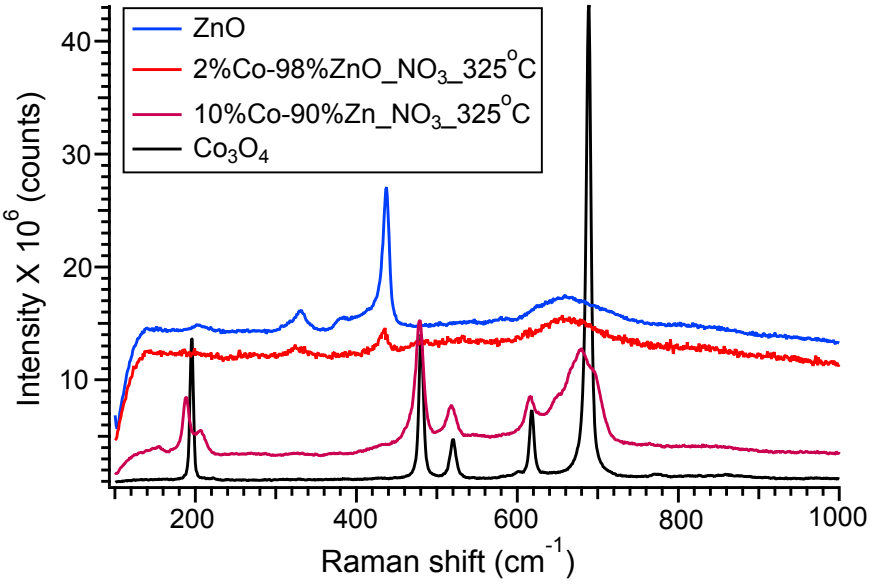

Figure 3.11: Raman spectra of Co-incorporated ZnO obtained from $Zn(NO_3)_2 \cdot 6\,H_2O$ and $Co(NO_3)_2 \cdot 6\,H_2O$ precursor, then dried at 325 °C. The presence of Co_3O_4 is not clear from the Raman spectra.

Raman spectra of Co-incorporated ZnO in Figure 3.11 shows the effect of heating on Co-incorporated ZnO with different concentrations. 2 wt.% of Co-incorporated ZnO has similar Raman spectra as in undoped ZnO. Heating at a higher temperature also did not confirm the presence of secondary phases in this sample. Co-incorporated ZnO sample containing 10 wt.% of cobalt precursor was heated at 325 °C and showed

the clear evidence of the formation of Co_3O_4 as a secondary phase. This was confirmed by Raman measurement, which consists characteristics Raman peaks of Co_3O_4 [86,87].

Co-incorporated ZnO prepared by using nitrate salts produces $Co(OH)_2$ and Co_3O_4 as secondary phases. A mixture of $ZnO/Co(OH)_2$ was found at a lower temperature, and at a higher temperature, it gives a mixture of ZnO/Co_3O_4. Nitrate salts do not help in the formation of secondary phase free Co-incorporated ZnO.

3.5 Summary of results

SSM reactions were performed to prepare a red light emitting Co-doped ZnO to use them in LEDs. Several other methods [38, 41] have been employed to prepare Co-doped ZnO, but very often secondary phases are formed during Co-doping into ZnO [107]. The approach was to prepare secondary phase free Co-doped ZnO. In order to achieve this goal, different precursor salts [94] and various concentrations of Co were tried. However, in each case, the Raman study confirmed the presence of secondary phase into Co-incorporated ZnO. One of the simple and direct approaches to confirm the emission property of phosphor materials is using UV light illumination in the dark environment. However, no evidence of emission of light was observed in these Co-incorporated ZnO samples. Since IR spectroscopy is also an important technique to obtain structural information, ATR spectra of Co-incorporated ZnO were measured. However, the measurement was not very helpful to detect the presence of secondary phases in the sample. This was due to the identical position of characteristic peaks for lattice vibrational mode of Zn and Co. Finally, UV-Vis reflectance spectroscopy was used to find the optical properties of Co-incorporated ZnO. The UV-Vis reflectance spectra of Co-incorporated ZnO shows the only peak due to the d-d electronic transition in Co^{2+} [33, 34, 96]. UV-Vis reflectance spectra did not show

any characteristic optical absorption of Co-doped ZnO. No significant shift of spectra was found in the band gap energy region, which made it difficult to detect a change in band gap energy due to the incorporation of Co into ZnO.

Chapter 4

Stoichiometric ZnO as part of a UV sensing device

ZnO materials are responsive to UV light. Due to this behaviour, ZnO can be used in UV sensing devices. The general description of UV sensitivity of ZnO is presented in Section 1.4.

The initial real-time photo-sensing response of UV illuminated ZnO films in the Poduska research group was investigated by Jiaqi Cheng, who was an earlier member of the group [50]. When DC voltage is applied to the ZnO film, the resistance decreases under UV exposure and increases when UV light is turned off. The same thing happens when a low frequency AC potential is applied: the impedance is higher in the dark than that under the influence of UV. In the case of a high-frequency AC potential, the impedance is higher under UV than in the dark. This crossing point that sets a threshold between low and high frequency plays an important role in determining the usability of ZnO as a UV sensor because it helps to identify the AC frequency range where exposure to UV light causes a decrease in impedance. The sensor can be calibrated based on the known frequency of the crossing point.

This study aimed to observe the frequency-dependent UV responses of ZnO to find what range of frequencies are low enough to behave like DC (UV exposure decreases impedance). The effect of humidity on this range of frequencies was also investigated.

4.1 Effect of humidity on photoresponsive behavior of ZnO films

The photoresponsive behavior of ZnO films was studied both for as-prepared films and after keeping films in an open dark box for several days with desiccants. Earlier studies reported that humidity affects the conductivity of ZnO films [50, 108, 109]. Thus, it is essential to control the moisture of ZnO films. After drying, films were stored in a dark box. To create a moisture free environment, activated desiccants were added to the box. Representative Nyquist plots are presented in Figure 4.1.

Figure 4.1 (a) shows a semicircle in the higher frequency (low Z_{re}) region and a tail in the lower frequency (high Z_{re}) region. Huang, Sappia and Tomer *et al.* [110–112] got the similar result when EIS spectra of ZnO films were measured under humid conditions. A 45° angle in the high Z_{re} region of the Nyquist plot corresponds to the Warburg impedance, providing evidence of water-like diffusion, which we equate with the presence of humidity in our ZnO films. The lack of a tail indicates a properly dried sample. Omri and Dridi *et al.* [113, 114] also studied EIS measurement of ZnO under dry condition and observed semicircles in the Nyquist plot.

The Bode plot of a properly dried ZnO film is presented in Figure 4.2 to compare responses under dark and UV illumination.

The comparison between UV and dark data in Figure 4.2 revealed that at lower frequencies, the impedance of the UV exposed sample is lower than when it is in the dark. For higher frequencies (above f_{cross}) this response is the opposite, which is

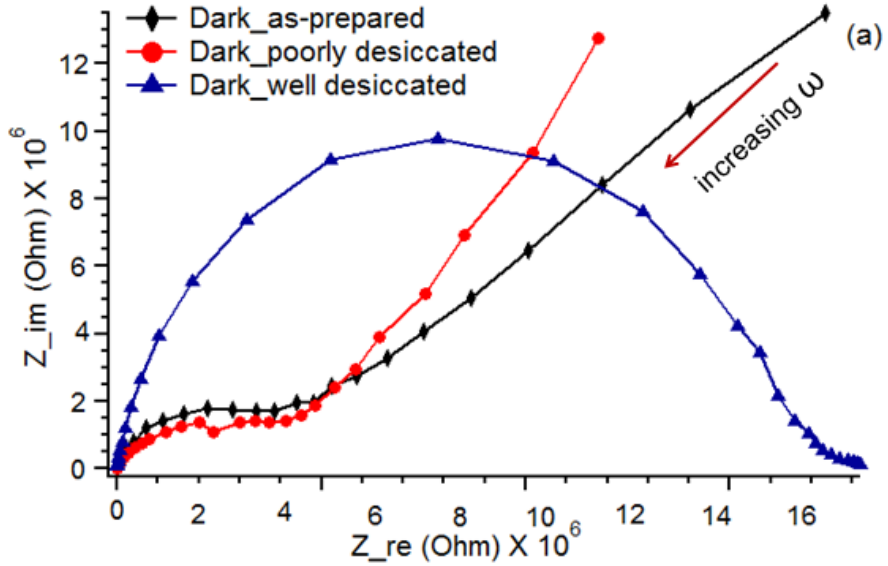

(a) Representative Nyquist plots of ZnO showing the effect of humidity change under dark conditions.

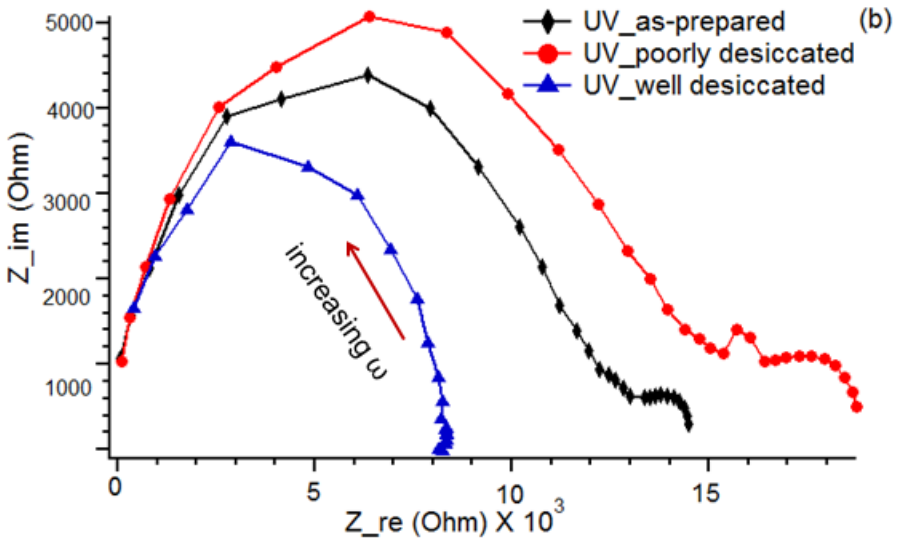

(b) Representative Nyquist plots of ZnO showing the humidity effect on the UV response.

Figure 4.1: Nyquist plot of a ZnO film measured under (a) dark and (b) UV conditions.

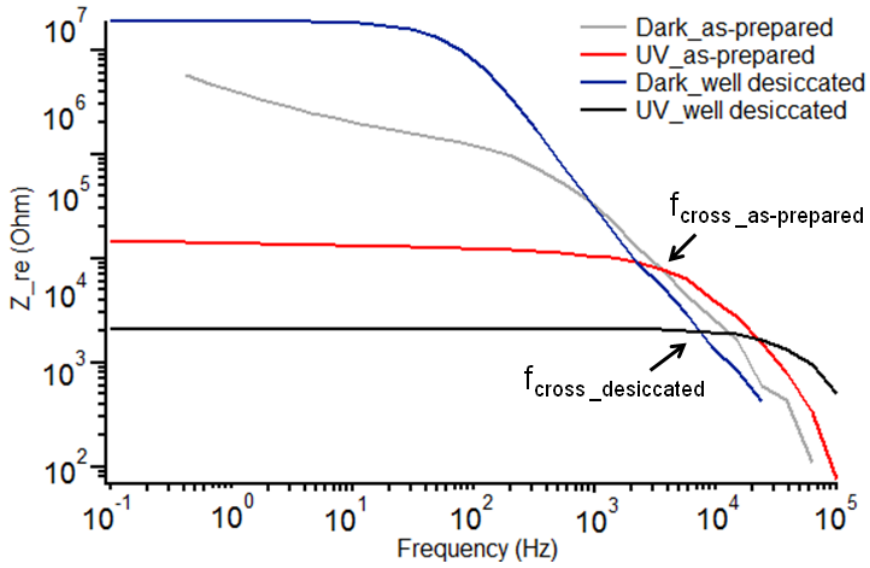

Figure 4.2: Representative Bode plot of a ZnO film, showing the location of f_{cross}.

consistent with the previous work from our group [50]. Hence, the sign and magnitude of the UV response depend on the frequency, and the impedance behavior of ZnO films determines the change of the sign.

Figure 4.2 also shows the changes in resistance and of f_{cross} of a ZnO film based on its exposure time to a humid environment. According to Yadav *et al.* [108], the resistance of a ZnO film can be determined by the amount of moisture adsorbed on the film. The film that was properly desiccated gives higher resistance than the as-prepared film. Although the percentage of humidity was not measured, the value of f_{cross} seems to depend on the level of humidity. A future study could be done based on the relationship of formation of f_{cross} with the percentage of humidity.

4.2 Frequency dependent photo-response of ZnO films and study of their reproducibilty

The photoresponsive behavior of ZnO films was observed by shining UV light on them. A recovery time is required after shining UV light, which was done by keeping the film in a dark box for five days. As after shining UV light on a film, it takes time to recover. Desiccants were used in the box to maintain a moisture-free environment.

Three samples (S1, S2, and S3) were prepared on ITO glass substrates using the same amounts of ZnO slurry. The substrates with the slurry were left in a fume-hood for drying which gave thin films of ZnO. The films were each sandwiched with a second pieces of ITO glass. A binder clip was used to keep the two ITO glass substrates together. These films were stored in a dark box with desiccants. The EIS measurements of those samples were carried out after different storing times: one day, two days and five days. For every different storing time, each sample was measured several times.

Three samples were compared with each other to see the location of f_{cross} values and how they vary from one sample to another. Based on the values found for different samples and storing times, error bars were calculated by plotting f_{cross} against time. It is useful to note that S1 is the same sample shown in Figure 4.1 and Figure 4.2.

Figure 4.3 shows that f_{cross} falls in a range of frequencies depending on samples and storing times. Sample 1 gave large error bars compared to others. Frequency-dependent photo-response of ZnO films is presented in a Bode plot, where values of resistance of different films can be determined as a function of frequency (Figure 4.4). In each case, the resistance is higher at lower frequencies and it starts to decrease at higher frequencies. Although the same measurement conditions were maintained for all three samples, there were resistance differences among the samples. The resistance

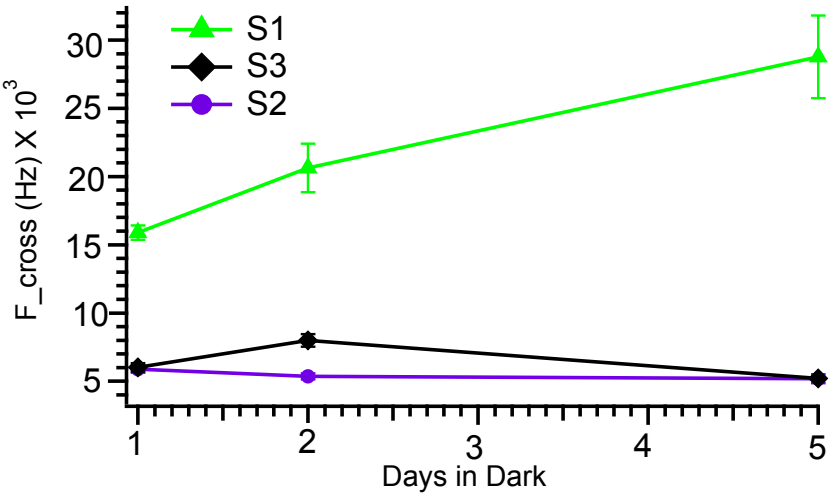

Figure 4.3: ZnO films showing the dependency of f_{cross} on different storing times.

of a ZnO film may be influenced by factors such as impurities, film thickness or the presence of NaCl by-product [50].

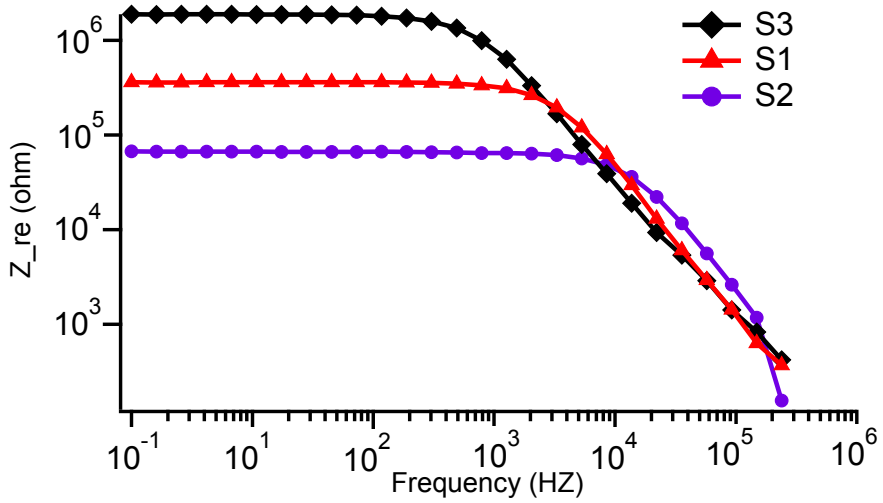

Figure 4.4: Bode plot of ZnO films, showing differences in resistance.

The presence of NaCl might affect the resistance of ZnO. Normally, the presence of NaCl in ZnO sample increases the resistivity because it has a higher resistance than ZnO. Since there were three different ZnO samples, the presence of NaCl might be different in different samples. The reason for this is that in order to prepare ZnO,

$ZnCl_2$ was used as a precursor salt. The reaction between $ZnCl_2$ and NaOH produces $Zn(OH)_2$ as an intermediate, where NaCl is produced as a by-product. This NaCl salt was removed with nanopure water. Further decomposition of $Zn(OH)_2$ produces ZnO and H_2O. Though NaCl was washed with water, a small amount of it may remain in ZnO sample.

It is observed in Figure 4.4 that the resistance of S1 is in between S2 and S3. Thus, it unlikely that it has more NaCl inclusions. Therefore, even though S1 had the largest error bars in Figure 4.3, it does not appear that a higher resistance (Z_{re} in Figure 4.4) is directly related to larger error bars.

4.3 Summary of results

Electrochemical impedance spectroscopy (EIS) measurements were performed to observe the UV response of ZnO films under applied AC potentials at many different frequencies. The impedance of the ZnO films was measured during UV exposure, darkness, and at different humidity levels.

In order to observe the reproduciblity of the frequency-dependent impedance behaviour, three films were prepared with a similar method and stored in the dark for different periods of time. EIS measurements of those samples showed that the impedance varies among different films. Although an equal amount of material was used to prepare each film, the thickness of those films could vary, which might be a reason for the difference in their impedance values. All properly dried films showed f_{cross}, but the values of f_{cross} varies somewhat among different films. Humidity also has an effect on the UV response of ZnO films.

Chapter 5

Conclusions

This thesis is devoted to studying the optical and electrical properties of ZnO, which is a well-known semiconductor. Selecting suitable phosphor materials that emit red light is crucial in tuning the properties of light obtained from white light emitting diodes (WLEDs). In this study, Co-incorporated ZnO was prepared through a solid state metathesis (SSM) reaction, so as to use it as a red-light-emitting phosphor. Raman spectra of Co-incorporated ZnO show evidence of $Co(OH)_2$ as a secondary phase. The spectra also confirm the conversion of $Co(OH)_2$ to Co_3O_4 at high temperature calcination. Different precursor salts were also used, but yielded similar results. The characteristic peaks for red emission were not found in the visible region of UV-Vis spectra. Hence, UV-Vis reflectance studies of Co-incorporated ZnO did not confirm Co-doping into ZnO.

Stoichiometric ZnO films were stored in the dark for different time periods and the frequency-dependent photoresponsive behavior of those films were studied using electrochemical impedance spectroscopy (EIS). From the EIS data, the dark and UV Bode spectra intersect each other at a certain frequency that we call f_{cross}. The level of humidity affects the value of f_{cross}, and those values vary among different samples.

Thus, calibration of these f_{cross} values would be necessary in order to use these films in a useful sensor.

Bibliography

[1] Y. Narukawa, M. Ichikawa, D. Sanga, M. Sano, and T. Mukai. White light emitting diodes with super-high luminous efficacy. *Journal of Physics D: Applied Physics*, 43(35):354002, 2010.

[2] C. Xu and K. M. Poduska. A bright future for color-controlled solid state lighting. *Journal of Materials Science: Materials in Electronics*, 26(7):4565–4570, 2015.

[3] Y. Li, F. Della Valle, M. Simonnet, I. Yamada, and J.-J. Delaunay. Competitive surface effects of oxygen and water on UV photoresponse of ZnO nanowires. *Applied Physics Letters*, 94(2):023110, 2009.

[4] C. C. Moura, R. S. Tare, R. O. C. Oreffo, and S. Mahajan. Raman spectroscopy and coherent anti-Stokes Raman scattering imaging: prospective tools for monitoring skeletal cells and skeletal regeneration. *Journal of The Royal Society Interface*, 13(118), 2016.

[5] C. M. Simonescu. *Application of FTIR Spectroscopy in Environmental Studies*, pages 60–65. InTech, 2012.

[6] C. Ronda. Challenges in application of luminescent materials, a tutorial overview (invited review). *Progress In Electromagnetics Research*, 147:81–93, 2014.

[7] P. Kumar, S. Singh, and B. K. Gupta. Future prospects of luminescent nanomaterial based security inks: from synthesis to anti-counterfeiting applications. *Nanoscale*, 8:14297–14340, 2016.

[8] Y. Hu, W. Zhuang, H. Ye, D. Wang, S. Zhang, and X. Huang. A novel red phosphor for white light emitting diodes. *Journal of Alloys and Compounds*, 390(1–2):226–229, 2005.

[9] H. Zhu, C. C. Lin, W. Luo, S. Shu, Z. Liu, Y. Liu, J. Kong, E. Ma, Y. Cao, R.-S. Liu, and X. Chen. Highly efficient non-rare-earth red emitting phosphor for warm white light-emitting diodes. *Nature Communications*, 5:4312, 2014.

[10] Z. Wang, Y. Zhou, Y. Liu, Q. Zhou, L. Luo, H. Tan, Q. Zhang, G. Chen, and J. Peng. Highly efficient red phosphor Cs_2GeF_6:Mn^{4+} for warm white light-emitting diodes. *RSC Advances*, 5:82409–82414, 2015.

[11] X. Huang. Solid-state lighting: Red phosphor converts white LEDs. *Nature Photonics*, 8(10):748–749, 2014.

[12] N. Boughen. *LightWave 3D 7.5 Lighting*, page 216. Wordware Publishing, Inc., 2003.

[13] B. Valeur and M. N. Berberan-Santos. A Brief History of Fluorescence and Phosphorescence before the Emergence of Quantum Theory. *Journal of Chemical Education*, 88(6):731–738, 2011.

[14] F. Clabau, X. Rocquefelte, T. Le Mercier, P. Deniard, S. Jobic, and M.-H. Whangbo. Formulation of Phosphorescence Mechanisms in Inorganic Solids Based on a New Model of Defect Conglomeration. *Chemistry of Materials*, 18(14):3212–3220, 2006.

[15] S. Kamiyama, M. Iwaya, T. Tetsuya, I. Akasaki, M. Syväjärvi, and R. Yakimova. Fluorescent SiC and its application to white light-emitting diodes. *Journal of Semiconductors*, 32(1):013004, 2011.

[16] A. Janotti and C. G. Van de Walle. Fundamentals of zinc oxide as a semiconductor. *Reports on Progress in Physics*, 72(12):126501, 2009.

[17] L. Schmidt-Mende and J. L. MacManus-Driscoll. ZnO - nanostructures, defects, and devices. *Materials Today*, 10(5):40–48, 2007.

[18] M.-H. Liu, Y.-W. Chen, X. Liu, J.-L. Kuo, M.-W. Chu, and C.-Y. Mou. Defect-Mediated Gold Substitution Doping in ZnO Mesocrystals and Catalysis in CO Oxidation. *ACS Catalysis*, 6(1):115–122, 2016.

[19] P. A. Rodnyi and I. V. Khodyuk. Optical and luminescence properties of zinc oxide (Review). *Optics and Spectroscopy*, 111(5):776–785, 2011.

[20] I. Djerdj, Z. Jaglicic, D. Arcon, and M. Niederberger. Co-Doped ZnO nanoparticles: Minireview. *Nanoscale*, 2:1096–1104, 2010.

[21] H. Zeng, G. Duan, Y. Li, S. Yang, X. Xu, and W. Cai. Blue Luminescence of ZnO Nanoparticles Based on Non-Equilibrium Processes: Defect Origins and Emission Controls. *Advanced Functional Materials*, 20(4):561–572, 2010.

[22] N. Bi, L. Zhang, Q. Zheng, F. Zhuge, J. Li, X. P. Gao, and J. Du. Control of ZnO nanowire growth and optical properties in a vapor deposition process. *Journal of Materials Science & Technology*, 33(8):850–855, 2017.

[23] A. S. Kamble, B. B. Sinha, K. Chung, M. G. Gil, V. Burungale, C.-J. Park, J. H. Kim, and P. S. Patil. Effect of hydroxide anion generating agents on growth and properties of ZnO nanorod arrays. *Electrochimica Acta*, 149:386–393, 2014.

[24] J. Kumar, S. Ramasubramanian, R. Thangavel, and M. Rajagopalan. *On the Optical and Magnetic Properties of Doped-ZnO*, pages 309–329. Springer India, 2014.

[25] P. Li, S. Wang, J. Li, and Y. Wei. Structural and optical properties of Co-doped ZnO nanocrystallites prepared by a one-step solution route. *Journal of Luminescence*, 132(1):220–225, 2012.

[26] Y. Zhu, G. Xu, G. Tengchao, H. Haili, and T. Shujuan. Preparation, infrared emissivity and thermochromic properties of Co doped ZnO by solid state reaction. *Journal of Alloys and Compounds*, 720:105–115, 2017.

[27] B. Wang, C. Xia, J. Iqbal, N. Tang, Z. Sun, Y. Lv, and L. Wu. Influences of Co doping on the structural, optical and magnetic properties of ZnO nanorods synthesized by hydrothermal route. *Solid State Sciences*, 11(8):1419–1422, 2009.

[28] J. H. Park, Y. J. Lee, J.-S. Bae, B.-S. Kim, Y. C. Cho, C. Moriyoshi, Y. Kuroiwa, S. Lee, and S.-Y. Jeong. Analysis of oxygen vacancy in Co-doped ZnO using the electron density distribution obtained using MEM. *Nanoscale Research Letters*, 10(1):186, 2015.

[29] K. E. Knutsen, A. Galeckas, A. Zubiaga, F. Tuomisto, G. C. Farlow, B. G. Svensson, and A. Y. Kuznetsov. Zinc vacancy and oxygen interstitial in ZnO revealed by sequential annealing and electron irradiation. *Physical Review B*, 86:121203, 2012.

[30] N. F. Djaja, D. A. Montja, and R. Saleh. The effect of Co incorporationinto ZnO nanoparticles. *Advances in Materials Physics and Chemistry*, 3(1):33–41, 2013.

[31] A. Kaushik, B. Dalela, R. Rathore, V. Vats, B. Choudhary, P. Alvi, S. Kumar, and S. Dalela. Influence of Co doping on the structural, optical and magnetic properties of ZnO nanocrystals. *Journal of Alloys and Compounds*, 578:328–335, 2013.

[32] M. Naeem, S. K. Hasanain, and A. Mumtaz. Electrical transport and optical studies of ferromagnetic cobalt doped ZnO nanoparticles exhibiting a metal–insulator transition. *Journal of Physics: Condensed Matter*, 20(2):025210, 2008.

[33] J. Hays, K. M. Reddy, N. Y. Graces, M. H. Engelhard, M. L. V Shutthanandan, C. Xu, N. C. Giles, C. Wang, S. Thevuthasan, and A. Punnoose. Effect of Co doping on the structural, optical and magnetic properties of ZnO nanoparticles. *Journal of Physics: Condensed Matter*, 19(26):266203, 2007.

[34] R. He, B. Tang, C. Ton-That, M. Phillips, and T. Tsuzuki. Physical structure and optical properties of Co-doped ZnO nanoparticles prepared by co-precipitation. *Journal of Nanoparticle Research*, 15(11):1–8, 2013.

[35] X.-C. Liu, E.-W. Shi, Z.-Z. Chen, H.-W. Zhang, L.-X. Song, H. Wang, and S.-D. Yao. Structural, optical and magnetic properties of Co-doped ZnO films. *Journal of Crystal Growth*, 296(2):135–140, 2006.

[36] M. A. García, F. Jiménez-Villacorta, A. Quesada, J. de la Venta, N. Carmona, I. Lorite, J. Llopis, and J. F. Fernández. Surface magnetism in ZnO/Co_3O_4 mixtures. *Journal of Applied Physics*, 107(4):043906, 2010.

[37] A. L. Dadlani, O. Trejo, S. Acharya, J. Torgersen, I. Petousis, D. Nordlund, R. Sarangi, P. Schindler, and F. B. Prinz. Exploring the local electronic structure

and geometric arrangement of ALD Zn(O,S) buffer layers using X-ray absorption spectroscopy. *Journal of Materials Chemistry C*, 3:12192–12198, 2015.

[38] V. Gandhi, R. Ganesan, H. H. A. Syedahamed, and M. Thaiyan. Effect of Cobalt Doping on Structural, Optical, and Magnetic Properties of ZnO Nanoparticles Synthesized by Coprecipitation Method. *The Journal of Physical Chemistry C*, 118(18):9715–9725, 2014.

[39] P. P. Sahay, S. Tewari, R. K. Nath, S. Jha, and M. Shamsuddin. Studies on ac response of zinc oxide pellets. *Journal of Materials Science*, 43(13):4534–4540, 2008.

[40] M. Arshad, A. Azam, A. S. Ahmed, S. Mollah, and A. H. Naqvi. Effect of Co substitution on the structural and optical properties of ZnO nanoparticles synthesized by sol–gel route. *Journal of Alloys and Compounds*, 509(33):8378–8381, 2011.

[41] M. K. Lima, D. M. Fernandes, M. F. Silva, M. L. Baesso, A. M. Neto, G. R. de Morais, C. V. Nakamura, A. de Oliveira Caleare, A. A. W. Hechenleitner, and E. A. G. Pineda. Co-doped ZnO nanoparticles synthesized by an adapted sol–gel method: effects on the structural, optical, photocatalytic and antibacterial properties. *Journal of Sol-Gel Science and Technology*, 72(2):301–309, 2014.

[42] J. Cheng, M. A. Rasheed, and K. M. Poduska. Exploiting Water-Mediated Ethanol Sensing by Polycrystalline ZnO at Room Temperature. *ECS Journal of Solid State Science and Technology*, 2(1):Q23–Q26, 2013.

[43] P. G. Devi and A. S. Velu. Synthesis, structural and optical properties of pure ZnO and Co doped ZnO nanoparticles prepared by the co-precipitation method. *Journal of Theoretical and Applied Physics*, 10(3):233–240, 2016.

[44] J. Xu, S. Shi, L. Li, X. Zhang, Y. Wang, Q. Shi, S. Li, and H. Wang. Luminescence Properties of Cobalt-Doped ZnO Films Prepared by Sol–Gel Method. *Journal of Electronic Materials*, 42(12):3438–3444, 2013.

[45] N. Coleman, P. Sujith, and E. G. Gillan. Rapid solid-state metathesis route to transition-metal doped titanias. *Journal of Solid State Chemistry*, 232:241–248, 2015.

[46] K. H. Lee, H. J. Jung, J. H. Lee, K. Kyungtae, B. Lee, D. Nam, C. M. Kim, M.-H. Jung, and N. H. Hur. Facile solid-state synthesis of oxidation-resistant metal nanoparticles at ambient conditions. *Solid State Sciences*, 79:38–47, 2018.

[47] C.-F. Jin, X. Yuan, W.-W. Ge, J.-M. Hong, and X.-Q. Xin. Synthesis of ZnO nanorods by solid state reaction at room temperature. *Nanotechnology*, 14(6):667, 2003.

[48] X. R. Ye, D. Z. Jia, J. Q. Yu, X. Q. Xin, and Z. Xue. One-Step Solid-State Reactions at Ambient Temperatures-A Novel Approach to Nanocrystal Synthesis. *Advanced Materials*, 11(11):941–942, 1999.

[49] M. A. Rasheed. *Synthesis, electrical and gas sensing properties of polycrystalline ZnO films*. PhD thesis, Memorial University of Newfoundland, 2012.

[50] J. Cheng. *Synthesis and surface reactivity of ZnO: application to gas and photon detection*. PhD thesis, Memorial University of Newfoundland, 2016.

[51] A. Muke, P. Muthal, S. Dhopte, and S. Moharil. Solid state metathesis of $CaSO_4$:Eu^{2+} phosphor. *Journal of Luminescence*, 132(2):342–344, 2012.

[52] R. S. Dariani and M. Zabihipour. Effect of electrical behavior of ZnO microparticles grown on porous silicon substrate. *Applied Physics A*, 122(12):1047, 2016.

[53] S. Inamdar, V. Ganbavle, and K. Rajpure. ZnO based visible - blind UV photodetector by spray pyrolysis. *Superlattices and Microstructures*, 76(Supplement C):253–263, 2014.

[54] T. Zhai, X. Fang, M. Liao, X. Xu, H. Zeng, B. Yoshio, and D. Golberg. A Comprehensive Review of One-Dimensional Metal-Oxide Nanostructure Photodetectors. *Sensors*, 9(8):6504–6529, 2009.

[55] K. Liu, M. Sakurai, and M. Aono. ZnO-Based Ultraviolet Photodetectors. *Sensors*, 10(9):8604–8634, 2010.

[56] L. Sang, M. Liao, and M. Sumiya. A Comprehensive Review of Semiconductor Ultraviolet Photodetectors: From Thin Film to One-Dimensional Nanostructures. *Sensors*, 13(8):10482–10518, 2013.

[57] L. Vikas, K. Vanaja, P. Subha, and M. Jayaraj. Fast UV sensing properties of n-ZnO nanorods/p-GaN heterojunction. *Sensors and Actuators A: Physical*, 242(Supplement C):116–122, 2016.

[58] D. Norton, Y. Heo, M. Ivill, K. Ip, S. Pearton, M. Chisholm, and T. Steiner. ZnO: growth, doping & processing. *Materials Today*, 7(6):34–40, 2004.

[59] S. Shaikh, V. Ganbavle, S. Mohite, and K. Rajpure. Chemical synthesis of pinecone like ZnO films for UV photodetector applications. *Thin Solid Films*, 642(Supplement C):232–240, 2017.

[60] C. Soci, A. Zhang, B. Xiang, S. A. Dayeh, D. P. R. Aplin, J. Park, X. Y. Bao, Y. H. Lo, , and D. Wang. ZnO Nanowire UV Photodetectors with High Internal Gain. *Nano Letters*, 7(4):1003–1009, 2007.

[61] L. Guo, H. Zhang, D. Zhao, B. Li, Z. Zhang, M. Jiang, and D. Shen. High responsivity ZnO nanowires based UV detector fabricated by the dielectrophoresis method. *Sensors and Actuators B: Chemical*, 166–167:12–16, 2012.

[62] Y. Li, F. D. Valle, M. Simonnet, I. Yamada, and J.-J. Delaunay. High-performance UV detector made of ultra-long ZnO bridging nanowires. *Nanotechnology*, 20(4):045501, 2009.

[63] Y. Xie, M. Madel, M. Feneberg, B. Neuschl, W. Jie, Y. Hao, X. Ma, and K. Thonke. Oxygen vacancies induced DX center and persistent photoconductivity properties of high quality ZnO nanorods. *Materials Research Express*, 3(4):045011, 2016.

[64] S. Tewari, A. Ghosh, and A. Bhattacharjee. Studies on frequency dependent electrical and dielectric properties of sintered zinc oxide pellets: effects of Al-doping. *Indian Journal of Physics*, 90(11):1247–1255, 2016.

[65] R. Martins, R. Igreja, I. Ferreira, A. Marques, A. Pimentel, A. Gonçalves, and E. Fortunato. Room temperature dc and ac electrical behaviour of undoped ZnO films under UV light. *Materials Science and Engineering: B*, 118(1–3):135–140, 2005.

[66] S. Panda and C. Jacob. Preparation of transparent ZnO thin films and their application in UV sensor devices. *Solid-State Electronics*, 73:44–50, 2012.

[67] P. P. Sahay, S. Tewari, S. Jha, and M. Shamsuddin. Sprayed ZnO thin films for ethanol sensors. *Journal of Materials Science*, 40(18):4791–4793, 2005.

[68] X. Qiu, R. Tang, J. Zhu, J. Oiler, C. Yu, Z. Wang, and H. Yu. The effects of temperature, relative humidity and reducing gases on the ultraviolet response

of ZnO based film bulk acoustic-wave resonator. *Sensors and Actuators B: Chemical*, 151(2):360–364, 2011.

[69] L. Lei and L. Zhang. Recent advance in high-pressure solid-state metathesis reactions. *Matter and Radiation at Extremes*, 3(3):95–103, 2018.

[70] F. A. Selim, M. H. Weber, D. Solodovnikov, and K. G. Lynn. Nature of Native Defects in ZnO. *Physical Review Letters*, 99:085502, 2007.

[71] D. Das and P. Mondal. Photoluminescence phenomena prevailing in c-axis oriented intrinsic ZnO thin films prepared by RF magnetron sputtering. *RSC Advances*, 4:35735–35743, 2014.

[72] M. Willander, O. Nur, N. Bano, and K. Sultana. Zinc oxide nanorod-based heterostructures on solid and soft substrates for white-light-emitting diode applications. *New Journal of Physics*, 11(12):125020, 2009.

[73] T. T. Loan, N. N. Long, and L. H. Ha. Photoluminescence properties of Co-doped ZnO nanorods synthesized by hydrothermal method. *Journal of Physics D: Applied Physics*, 42(6):065412, 2009.

[74] J. Cheng and K. M. Poduska. Ambient Degradation of ZnO Powders: Does Surface Polarity Matter? *ECS Journal of Solid State Science and Technology*, 3(5):P133–P137, 2014.

[75] C. Lai, X. Wang, Y. Zhao, H. Fong, and Z. Zhu. Effects of humidity on the ultraviolet nanosensors of aligned electrospun ZnO nanofibers. *RSC Advances*, 3:6640–6645, 2013.

[76] G. S. Bumbrah and R. M. Sharma. Raman spectroscopy – Basic principle, instrumentation and selected applications for the characterization of drugs of abuse. *Egyptian Journal of Forensic Sciences*, 6(3):209–215, 2016.

[77] A. Cantarero. Raman Scattering Applied to Materials Science. *Procedia Materials Science*, 9:113–122, 2015.

[78] Q. Cao, S. He, Y. Deng, D. Zhu, X. Cui, G. Liu, H. Zhang, S. Yan, Y. Chen, and L. Mei. Raman scattering investigations on Co-doped ZnO epitaxial films: Local vibration modes and defect associated ferromagnetism. *Current Applied Physics*, 14(5):744–748, 2014.

[79] A. Sacco. Electrochemical impedance spectroscopy: Fundamentals and application in dye-sensitized solar cells. *Renewable and Sustainable Energy Reviews*, 79(Supplement C):814–829, 2017.

[80] Z. Aljabal. Dielectric spectroscopy of organic solvents of varying polarity. Master's thesis, Memorial University of Newfoundland, 2016.

[81] D. Ribeiro and J. Abrantes. Application of electrochemical impedance spectroscopy (EIS) to monitor the corrosion of reinforced concrete: A new approach. *Construction and Building Materials*, 111:98–104, 2016.

[82] T. Ren, H. R. Baker, and K. M. Poduska. Optical absorption edge shifts in electrodeposited ZnO thin films. *Thin Solid Films*, 515(20–21):7976–7983, 2007.

[83] K. Samanta, A. K. Arora, and R. S. Katiyar. Local vibrational modes and Fano interaction in p-type ZnO:Sb system. *Journal of Physics D: Applied Physics*, 45(18):185304, 2012.

[84] K. Samanta, P. Bhattacharya, R. S. Katiyar, W. Iwamoto, P. G. Pagliuso, and C. Rettori. Raman scattering studies in dilute magnetic semiconductor, ZnCoO. *Physical Review B*, 73:245213, 2006.

[85] J. A. Koza, C. M. Hull, Y.-C. Liu, and J. A. Switzer. Deposition of $Co(OH)_2$ Films by Electrochemical Reduction of Tris(ethylenediamine)cobalt(III) in Alkaline Solution. *Chemistry of Materials*, 25(9):1922–1926, 2013.

[86] S. Deng, N. Chen, D. Deng, Y. Li, X. Xing, and Y. Wang. Meso- and macroporous coral-like Co_3O_4 for VOCs gas sensor. *Ceramics International*, 41(9, Part A):11004–11012, 2015.

[87] M. Figlarz, J. Guenot, and F. Fievet-Vincent. Morphological and topotactical aspects of the reactions $Co(OH)_2$ CoOOH and CoOOH Co_3O_4. *Journal of Materials Science*, 11(12):2267–2270, 1976.

[88] J. Yang, H. Hyodo, K. Kimura, and T. Sasaki. $Co(OH)_3$ nanobelts: synthesis, characterization and shape-preserved transformation to pseudo-single-crystalline Co_3O_4 nanobelts. *Nanotechnology*, 21(4):045605, 2010.

[89] L. M. Alrehaily, J. M. Joseph, M. C. Biesinger, D. A. Guzonas, and J. C. Wren. Gamma-radiolysis-assisted cobalt oxide nanoparticle formation. *Physical Chemistry Chemical Physics*, 15:1014–1024, 2013.

[90] B. G. Choi, M. Yang, S. C. Jung, K. G. Lee, J.-G. Kim, H. Park, T. J. Park, S. B. Lee, Y.-K. Han, and Y. S. Huh. Enhanced Pseudocapacitance of Ionic Liquid/Cobalt Hydroxide Nanohybrids. *ACS Nano*, 7(3):2453–2460, 2013.

[91] J. H. Nguyen, M. B. Kruger, and R. Jeanloz. Compression and pressure-induced amorphization of $Co(OH)_2$ characterized by infrared vibrational spectroscopy. *Physical Review B*, 49:3734–3738, 1994.

[92] M. Herrero, P. Benito, F. Labajos, and V. Rives. Nanosize cobalt oxide-containing catalysts obtained through microwave-assisted methods. *Catalysis Today*, 128(3–4):129–137, 2007.

[93] Y. Li, W. Qiu, F. Qin, H. Fang, V. G. Hadjiev, D. Litvinov, and J. Bao. Identification of Cobalt Oxides with Raman Scattering and Fourier Transform Infrared Spectroscopy. *The Journal of Physical Chemistry C*, 120(8):4511–4516, 2016.

[94] R. Bhargava, P. K. Sharma, S. Kumar, A. C. Pandey, and N. Kumar. Raman investigations of $Zn_{1-x}Co_xO$ nanocrystals: role of starting precursors on vibrational properties. *Journal of Raman Spectroscopy*, 42(9):1802–1807, 2011.

[95] Y.-C. Liu, J. A. Koza, and J. A. Switzer. Conversion of electrodeposited $Co(OH)_2$ to CoOOH and Co_3O_4, and comparison of their catalytic activity for the oxygen evolution reaction. *Electrochimica Acta*, 140:359–365, 2014.

[96] J. El Ghoul, M. Kraini, and L. El Mir. Synthesis of Co-doped ZnO nanoparticles by sol-gel method and its characterization. *Journal of Materials Science: Materials in Electronics*, 26(4):2555–2562, 2015.

[97] S. Colis, H. Bieber, S. Bégin-Colin, G. Schmerber, C. Leuvrey, and A. Dinia. Magnetic properties of Co-doped ZnO diluted magnetic semiconductors prepared by low-temperature mechanosynthesis. *Chemical Physics Letters*, 422:529–533, 2006.

[98] X. Liu, E. W. Shi, Z. Z. Chen, H. W. Zhang, B. Xiao, and L. X. Song. High-temperature ferromagnetism in (Co, Al)-codoped ZnO powders. *Applied Physics Letters*, 88(25):252503–3, 2006.

[99] S. Ekambaram. Combustion synthesis and characterization of new class of ZnO-based ceramic pigments. *Journal of Alloys and Compounds*, 390(1–2):L4–L6, 2005.

[100] L. Yan, C. K. Ong, and X. S. Rao. Magnetic order in Co-doped and (Mn, Co) codoped ZnO thin films by pulsed laser deposition. *Journal of Applied Physics*, 96(1):508–511, 2004.

[101] J. Cunha, D. Melo, A. Martinelli, M. Melo, I. Maia, and S. Cunha. Ceramic pigment obtained by polymeric precursors. *Dyes and Pigments*, 65(1):11–14, 2005.

[102] S. Rasouli and S. J. Moeen. Combustion synthesis of Co-doped zinc oxide nanoparticles using mixture of citric acid–glycine fuels. *Journal of Alloys and Compounds*, 509(5):1915–1919, 2011.

[103] M. Gaudon, O. Toulemonde, , and A. Demourgues. Green Coloration of Co-Doped ZnO Explained from Structural Refinement and Bond Considerations. *Inorganic Chemistry*, 46(26):10996–11002, 2007.

[104] M. S. Inpasalini, P. V. Rajesh, D. Das, and S. Mukherjee. Structural, optical and magnetic studies of co-doped mesoscopic ZnO nanoparticles. *Journal of Materials Science: Materials in Electronics*, 26(2):1053–1059, 2015.

[105] Y. Chang, P. Wang, S. Ni, Y. Long, and X. Li. Influence of Co Content on Raman and Photoluminescence Spectra of Co Doped ZnO Nanowires. *Journal of Materials Science & Technology*, 28(4):313–316, 2012.

[106] L. L. Zhao, J. Y. Wang, X. L. Wang, Z. X. Cheng, J. Wang, N. Yin, Z. G. Gai, A. Jalalian, and S. X. Dou. Cobalt doping effects on photoluminescence,

Raman scattering, crystal structure, and magnetic and piezoelectric properties in ZnO single crystals grown from molten hydrous LiOH and NaOH solutions. *Journal of Alloys and Compounds*, 628:303–307, 2015.

[107] X. Wang, R. Zheng, Z. Liu, H. pui Ho, J. Xu, and S. P. Ringer. Structural, optical and magnetic properties of Co-doped ZnO nanorods with hidden secondary phases. *Nanotechnology*, 19(45):455702, 2008.

[108] B. Yadav, R. Srivastava, C. Dwivedi, and P. Pramanik. Moisture sensor based on ZnO nanomaterial synthesized through oxalate route. *Sensors and Actuators B: Chemical*, 131(1):216–222, 2008.

[109] C.-L. Hsu, L.-F. Chang, and T.-J. Hsueh. Light-activated humidity and gas sensing by ZnO nanowires grown on LED at room temperature. *Sensors and Actuators B: Chemical*, 249(Supplement C):265–277, 2017.

[110] J. Huang, Z. Yang, Z. Feng, X. Xie, and X. Wen. A novel ZnO@Ag@Polypyrrole hybrid composite evaluated as anode material for zinc-based secondary cell. *Scientific Reports*, 6:24471, 2016.

[111] L. D. Sappia, M. R. Trujillo, I. Lorite, R. E. Madrid, M. Tirado, D. Comedi, and P. Esquinazi. Nanostructured ZnO films: A study of molecular influence on transport properties by impedance spectroscopy. *Materials Science and Engineering: B*, 200:124–131, 2015.

[112] V. K. Tomer, S. Duhan, A. K. Sharma, R. Malik, S. Nehra, and S. Devi. One pot synthesis of mesoporous ZnO–SiO_2 nanocomposite as high performance humidity sensor. *Colloids and Surfaces A: Physicochemical and Engineering Aspects*, 483:121–128, 2015.

[113] K. Omri, I. Najeh, and L. E. Mir. Influence of annealing temperature on the microstructure and dielectric properties of ZnO nanoparticles. *Ceramics International*, 42(7):8940–8948, 2016.

[114] R. Dridi, I. Saafi, A. Mhamdi, A. Matri, A. Yumak, M. H. Lakhdar, A. Amlouk, K. Boubaker, and M. Amlouk. Structural, optical and AC conductivity studies on alloy ZnO–Zn_2SnO_4 (ZnO–ZTO) thin films. *Journal of Alloys and Compounds*, 634:179–186, 2015.